Geomechanics and Engineering, *Vol. 34, No. 4 (2023) 341-380*
https://doi.org/10.12989/gae.2023.34.4.341

Seismic fragility assessments of fill slopes in South Korea using finite element simulations

Dung T.P. Tran[a], Youngkyu Cho[b], Hwanwoo Seo[c] and Byungmin Kim*

Department of Urban and Environmental Engineering, Ulsan National Institute of Science and Technology, 50, UNIST-gil, Eonyang-eup, Ulju-gun, Ulsan 44919, Republic of Korea

(*Received March 3, 2023, Revised May 16, 2023, Accepted June 27, 2023*)

Abstract. This study evaluates the seismic fragilities in fill slopes in South Korea through parametric finite element analyses that have been barely investigated thus far. We consider three slope geometries for a slope of height 10 m and three slope angles, and two soil types, namely frictional and frictionless, associated with two soil states, loose and dense for frictional soils and soft and stiff for frictionless soils. The input ground motions accounting for four site conditions in South Korea are obtained from one-dimensional site response analyses. By comparing the numerical modeling of slopes using PLAXIS^{2D} against the previous studies, we compiled suites of the maximum permanent slope displacement (D_{max}) against two ground motion parameters, namely, peak ground acceleration (PGA) and Arias Intensity (I_A). A probabilistic seismic demand model is adopted to compute the probabilities of exceeding three limit states (minor, moderate, and extensive). We propose multiple seismic fragility curves as functions of a single ground motion parameter and numerous seismic fragility surfaces as functions of two ground motion parameters. The results show that soil type, slope angle, and input ground motion influence these probabilities, and are expected to help regional authorities and engineers assess the seismic fragility of fill slopes in the road systems in South Korea.

Keywords: fill slope; finite element analysis; ground motion characteristic; seismic fragility assessment; site conditions; slope angle

1. Introduction

Civil infrastructures generally exist alongside slopes, such as dams, roadway embankments, bridge abutment systems, and lifeline systems crossing the mountains. Slope failures or landslides have been reported during several earthquakes in the past decades. For instance, the 2018 Hokkaido Eastern Iburi earthquake with a moment magnitude (**M**) of 6.6 resulted in a large number of slope failures near the towns of Atsuma, Mukawa, and Abira in Japan. Shallow landslides with volumes of approximately 23–38 × 10^6 m^3 occurred due to this earthquake (Wang *et al.* 2019). Chen *et al.* (2012) studied earthquake-induced chain disasters (e.g., landslides and debris flows) caused by the 2008 **M**7.9 Wenchuan earthquake in China. On September 21, 1999, the Chi-Chi earthquake with **M**7.7 triggered landslides on the dip slope at the Chiufengershan and formed two landslide-dammed lakes in Taiwan (Shou and Wang 2003). These case histories indicate the importance of assessing the hazards associated with earthquake-induced slope movements. According to Wei *et al.* (2022), the 2008 Wenchuan earthquake in China triggered widespread landslides that inflicted severe damage to the transportation infrastructure, including roads and railways, resulting in disruptions and delayed delivery of goods. National planning commission (Nepal 2015) estimated that the economic losses from the earthquake and associated landslides amounted to around $86 billion, with transportation and supply chains disruptions accounting for a considerable portion of these losses. Furthermore, earthquake-induced landslides can cause significant damage to the environment, including soil erosion, deforestation, and loss of biodiversity. This can have long-term impacts on the ecosystem and the surrounding communities (Schuster and Highland 2001).

Empirical relationships between the seismic demand (D) of slopes (e.g., permanent seismic slope displacement) and ground motion parameters (GMPs) [e.g., peak ground acceleration (PGA)] have been widely developed through various approaches such as pseudo-static calculation and numerical simulation for the seismic fragility assessment of slopes. Zhang *et al.* (2012) performed a numerical simulation of a slope based on a tension-shear failure mechanism using FLAC^{3D}. The slope model had a height of 20 m and a slope angle of 45° and was subjected to a ground motion record from the 1997 **M**6.9 Kobe earthquake. The simulation indicated a permanent displacement of 28.96 cm with a factor of safety of 0.98 and a continuous failure surface expanding slowly from the slope toe to the slope top. They also confirmed that the simulation-derived continuous failure surface was comparable with traditional failure mechanisms (Newmark's method). The resulting factor of safety (0.98), based on the tension-shear failure mechanism, decreased by

*Corresponding author, Associate Professor
E-mail: byungmin.kim@unist.ac.kr
[a]Ph.D. Student
[b]Research Professor
[c]Ph.D. Student

ISSN: 2005-307X (Print), 2092-6219 (Online)

12% compared to the traditional failure mechanism (1.11). Using FLAC^{2D}, Fotopoulou and Pitilakis (2015) performed numerical parametric analyses for evaluating earthquake-induced slope displacements against various GMPs such as PGA, peak ground velocity (PGV), and Arias Intensity (I_A). They considered multiple slope models [two slope heights = 20 m and 40 m, three slope angle = 15°, 30°, and 45°, and three values of shear wave velocity (V_S) = 150, 250, and 400 m/s] as representatives of general slope materials (frictional and frictionless soils), and a suite of acceleration records (40) that covered PGA between 0.065 g and 0.91 g from earthquakes with **M** ranging between 5 and 7.62. Based on the results from the numerous simulations, they derived a relationship between the earthquake-induced slope displacements and GMP (e.g., PGA, PGV, or I_A) that is widely applicable to earthquake engineering practices. An extensive review of seismic slope stability can be found in the literature (Crowley *et al.* 2004, Kim and Sitar 2013, Saygili and Rathje 2009, Tsompanakis *et al.* 2010, Zhang *et al.* 2012).

Currently, the seismic vulnerability of slopes is being evaluated by developing fragility curves, which describe the conditional probability of exceeding a limit state against GMP. Maruyama *et al.* (2010) presented fragility curves for expressway embankments based on a dataset of damages compiled from expressways in Japan. These embankment damages occurred during four earthquakes, namely the 2003 **M**6.2 Northern-Miyagi, 2003 **M**8.3 Tokachi-oki, and 2004 **M**6.6 Niigata Chuetsu. They considered embankment heights ranging from 5 to 10 m and investigated five levels of the seismic capacity limit state (very minor, minor, moderate, major, and severe) to develop the fragility curves with respect to PGV. Wu (2014) developed fragility curves for typical fill slopes subjected to multiple input motions by considering different failure mechanisms (e.g., shallow sliding of the infinite slope, circular slip surface of a homogeneous slope, and tetrahedral wedge failure in a rock slope). They utilized the lognormal cumulative distribution function (CDF) to simplify the empirical fragility curves. Soil properties and slope geometries have a significant impact on the fragility curves. A higher probability of exceedance is associated with an increase in the slope height and inclination. Slopes with soft soil properties [where cohesion (c) and friction angle (ϕ) are small] show a higher probability of exceedance than those with stiff soil properties (those having large c and ϕ). Hu *et al.* (2019) proposed seismic fragility functions for slopes, based on incremental dynamic analysis. They developed a soil slope model with a height of 20 m and a horizontal length of 70 m. Acceleration records (50) from the Pacific Earthquake Engineering Research (PEER) ground motion database were used as input motions. Five threshold values describing the states of vulnerability (unacceptable, minor, moderate, sufficient, and very sufficient) were selected from five levels of safety factors (1, 1.25, 1.4, 2.0, and 2.5), which correspond to five safety margins (none, low, moderate, high, and very high). Fragility curves were obtained from the CDF with respect to PGA. The probabilities of exceeding the different states of vulnerability increase with the increasing safety margins. Consequently, the seismic fragility assessments considering various factors (e.g., slope geometry, slope material properties and site condition) can enhance the seismic performance and help mitigate damages from future earthquakes; thereby, it can contribute to the resilience of a community by enabling a prompt and effective response to the earthquake-induced damages (EERI, 2010; El-Maissi *et al.*, 2020).

This study investigates the seismic fragility of fill slopes in South Korea through numerous finite element simulations using PLAXIS^{2D}. We consider 12 slope models that consist of a slope height (H_{slope}) = 10 m with varying slope angles (β) = 20°, 30°, and 40°, two soil types (frictional and frictionless soils), and two states of soils (loose and dense for frictional, and soft and stiff for frictionless). We use 280 input motions that account for four site conditions in South Korea (Kim *et al.* 2018). We conduct 5,040 nonlinear time-history analyses to compute suites of maximum permanent slope displacement (D_{max}) on the slope surfaces. Based on the results, we develop the probabilistic seismic demand model (PSDM) to compute the conditional probability (seismic fragility curves or fragility surfaces) of the D of slopes exceeding a certain limit state for a given level of a ground motion parameter (e.g., PGA or I_A).

2. Ground motion set

The responses of systems subjected to the earthquake loadings are remarkably influenced by the stochastic characteristics of ground shaking (Anderson *et al.* 2009, Argyroudis *et al.* 2013, Erberik 2015, Jafarian and Miraei 2019, Lee *et al.* 2020, McKenna *et al.* 2021, Newmark 1965, Raghunandan and Liel 2013, Varnier and Hatami 2011, Wu 2014, Zamiran and Osouli 2018, Zhang *et al.* 2018). More than seven ground motion records are generally required to assess the seismic fragility of structural systems (BSSC 2000, CEN 2004, Chiou *et al.* 2011, Zamiran and Osouli 2018, Zhang *et al.* 2016). In this study, we selected seven pairs of rock outcrop motions (14 records). Each pair comprises both north-south (NS) and east-west (EW) components recorded at rock outcrops. Two pairs of records were compiled from the two latest major earthquakes in South Korea (the 2016 **M**5.5 Gyeongju and 2017 **M**5.4 Pohang earthquakes) provided by the National Earthquake Comprehensive Information System. The remaining five pairs of records from earthquakes in other countries (Japan, U.S.A, Greece, and Italy) were collected from the Kiban-Kyoushin network and PEER center. The detailed information on selected earthquakes is presented in Table 1. **M** ranges from 5.4–6.7, and the distances are smaller than 40 km. These rock outcrop ground motions were recorded at the sites with average shear wave velocities on the top of a 30 m deposit (V_{S30}) being greater than or equal to 650 m/s. It is worth noting that these rock outcrop ground motions cover a wide range of characteristics (PGA: 0.11–0.41 g, Mean Period (T_m): 0.12–0.48 s, and 5–95% Significant Duration ($D_{5\text{-}95\%}$): 2.05–12.91 s). Fig. 1 shows the 5% damped acceleration response

Table 1 Earthquakes considered for selecting the seven pairs of rock outcrop ground motions

No.	Earthquake (Country, Year)	Moment magnitude (**M**)	Distance (km)	V_{S30} (m/s)	Direction	PGA (g)	I_A (m/s)
1	Gyeongju (Korea, 2016)	5.5	9.1*	797	EW	0.41	2.20
					NS	0.34	2.12
2	Pohang (Korea, 2016)	5.4	9.5*	815	EW	0.24	0.33
					NS	0.29	0.31
3	Hokkaido (Japan, 2018)	6.7	34.0*	1027	EW	0.13	0.24
					NS	0.12	0.21
4	N.Palm Springs (USA, 1986)	6.1	17.0**	659	EW	0.13	0.28
					NS	0.11	0.15
5	Kozani Greece-01 (Greece, 1995)	6.4	19.5**	650	EW	0.21	0.37
					NS	0.14	0.22
6	Sierra Madre (USA, 1991)	5.6	10.4**	680	EW	0.19	0.48
					NS	0.28	0.69
7	L'Aquila Italy (Italy, 2009)	5.6	15.0**	685	EW	0.13	0.14
					NS	0.11	0.14

*Epicentral distance.
**Rupture distance.

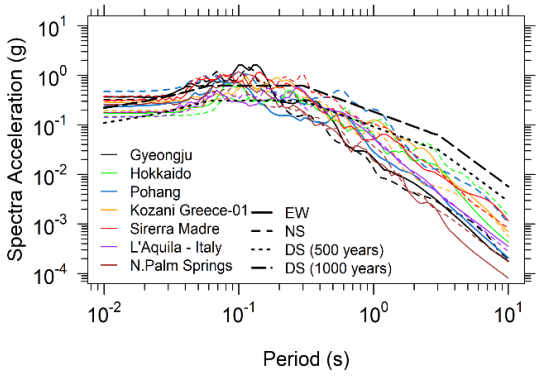

Fig. 1 The 5% damped acceleration response spectra of the selected 14 rock outcrop motions used in this study that are compatible with the Korean design response spectra (Seo *et al.* 2022)

spectra of the 14 selected rock outcrop ground motions. As the local site condition significantly changes the ground motion characteristics, we considered four site conditions (i.e., S2, S3, S4, and S5) suitable for South Korea based on site classification system (Kim *et al.*, 2018). The details of the site response analyses are described in Seo *et al.* (2022). The site response analyses produced four types of input ground motions (M2, M3, M4, and M5) for the numerical simulation of slopes that represent shallow/stiff, shallow/soft, deep/stiff, and deep/soft site conditions, respectively. Table 2 lists the range of values for the ground motions parameters for the four site conditions. The 14 records for each type from the site response analyses were scaled to five PGA levels of 0.1 g, 0.3 g, 0.5 g, 0.7 g, and 0.9 g. We eventually compiled 280 input ground motions (14 rock outcrop records × four site conditions × five PGA levels) for the numerical simulation.

3. Numerical simulations

We performed numerical simulations using the finite element software, PLAXIS^{2D} (PLAXIS-Manual, 2022). The subsequent sections describe the slope geometry, model verification, and nonlinear time history analyses.

3.1 Slope modeling

3.1.1 Slope geometry

We considered slopes with H_{slope} = 10 m and three β (= 20°, 30°, and 40°) for nonlinear time history analyses, as shown in Fig. 2. A depth of 10 m below the H_{slope} is provided to allow a slip surface to form below the slope toe. We also divided the entire height of the slope of the models into four sublayers to account for the effect of confining pressure on the modulus reduction and damping ratio curves. The slope geometries of interest correspond to fill slopes that generally exist in the road system. Park *et al.* (2018) evaluated a case study on seismic slope stability caused by the 2017 Gyeongju earthquake in South Korea, where they considered H_{slope} = 16 m and β ranging from 30° to 45°. Park and Cho (2017) analyzed the seismic fragility of cut slopes where they performed the Newmark sliding block approach with the H_{slope} approximately ranging from 5 to 15 m and β approximately ranging from 15° to 40°. Based on these reviews of the literature, we developed slope models with H_{slope} = 10 m, 30°, and 40° for the purpose of this study.

3.1.2 Material properties of slope model and motion type

We considered two soil types (frictional and frictionless soils) for the slope models based on strength parameters. The frictional soil is represented by the c – ϕ strength type, whereas ϕ = 0 strength type [c = undrained shear strength (S_u)] is selected for describing frictionless soils.

Table 2 Ranges values of ground motion parameters for each set of ground motions

Ground motion types/ GMPs	M2		M3		M4		M5	
	Min	Max	Min	Max	Min	Max	Min	Max
PGA (g)	0.1	0.9	0.1	0.9	0.1	0.9	0.1	0.9
PGV (cm/s)	1.96	48.54	1.14	68.70	0.73	55.84	1.85	75.39
PGD (cm)	0.06	10.45	0.22	10.30	0.09	9.01	0.30	19.06
I_A (m/s)	0.02	8.34	0.04	15.93	0.03	10.04	0.05	11.62
CAV (cm/s)	32.60	1821.08	83.29	2804.46	38.44	2022.77	63.27	2497.00
T_m (s)	0.10	0.36	0.16	0.59	0.13	0.43	0.17	0.80
$D_{S5\text{-}95}$ (s)	1.15	8.21	1.48	9.59	0.83	8.33	1.41	12.06

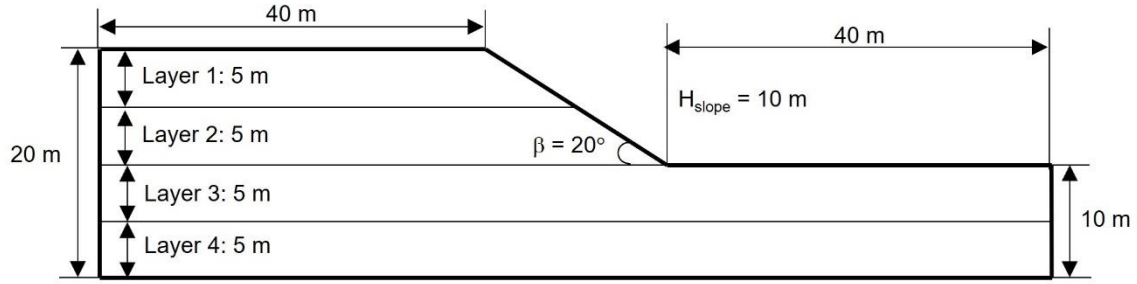

(a) β = 20°

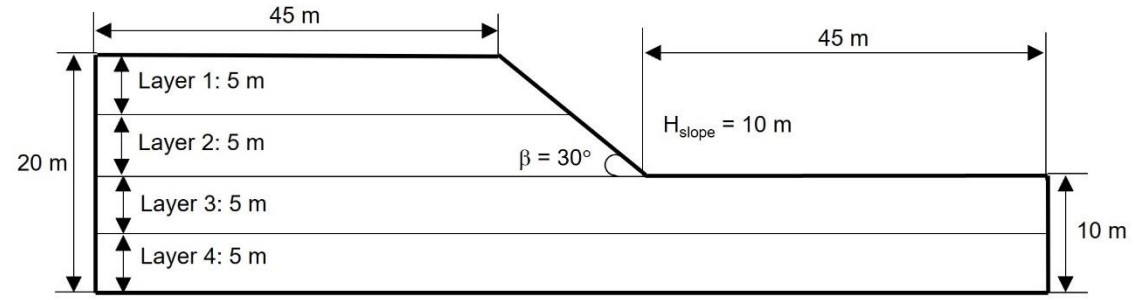

(b) β = 30°

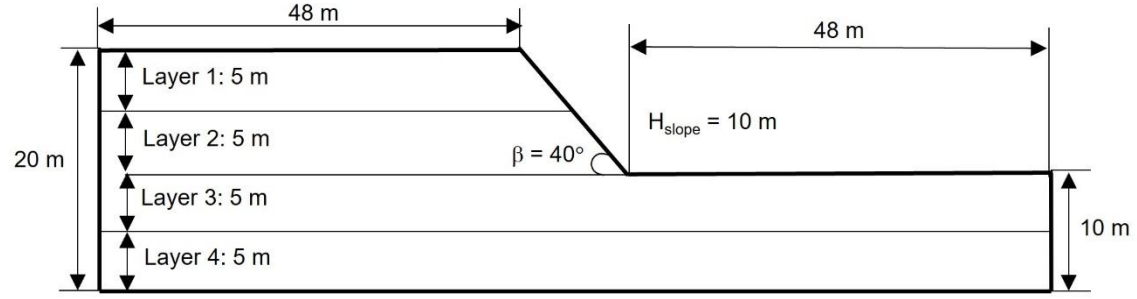

(c) β = 40°

Fig. 2 Representative geometries for modeling fill slopes with three β

Table 3 lists the strength parameters of the slope models along with the geometrical parameters of the slope (H_{slope} and β) and the associated types of input ground motions.

The material properties assigned to the three slope geometries comprise We considered two soil types (frictional and frictionless soils) for the slope models based on strength parameters. The frictional soil is represented by the c – ϕ strength type, whereas ϕ = 0 strength type [c = undrained shear strength (S_u)] is selected for describing frictionless soils. Table 3 lists the strength parameters of the slope models along with the geometrical parameters of the slope (H_{slope} and β) and the associated types of input ground motions. The material properties assigned to the three slope geometries comprise the frictional and frictionless soils that are coupled with two values of the V_S (150 m/s and 300 m/s) that account for the two states of the soils, such as the loose and dense states for frictional soils and the soft and stiff states for frictionless soils. For the

Table 3 Geometry of the slope models, soil properties, ground motion types considered in this study

H_{slope} (m)	Slope angle, β (°)	Soil strength type	V_S (m/s)	k_y (g)	Unit weight, γ_t (kN/m^3)	Friction angle, ϕ(°)	c or S_u (kPa)	Input ground motion type
10	20 30 40	c - ϕ (Frictional)	150 (Loose)	β = 20°, 0.438 β = 30°, 0.332 β = 40°, 0.225	17	30	10	M2, M3, M4, M5.
			300 (Dense)	β = 20°, 0.611 β = 30°, 0.481 β = 40°, 0.354	20	40		M2, M4.
		ϕ = 0 (Frictionless)	150 (Soft)	β = 20°, 0.183 β = 30°, 0.191 β = 40°, 0.186	17	0	48	M2, M3, M4, M5.
			300 (Stiff)	β = 20°, 0.301 β = 30°, 0.327 β = 40°, 0.322	20		72	M2, M4.

frictional soils, we considered two friction angles (ϕ = 30° and 40°) from the two relative densities of sand (loose and dense) based on the empirical relationship between the SPT-N value and the relative density of sand derived by Terzaghi and Peck (1967). For instance, the SPT-N values range from 4 to 10 for loose frictional soils that pertain to ϕ in the range of 30–35°.

To take into account conservative estimation, we selected ϕ = 30° for loose frictional soils and ϕ = 40° for dense frictional soils. We approximated the corresponding V_S to be 150 m/s and 300 m/s, respectively, for these two frictional soils using the empirical relationship between V_S and SPT-N developed for Korean sites [V_S (m/s) = $65.64 \cdot N^{0.407}$ for all soil types proposed by Sun *et al.* (2012)]. Additionally, we used c = 10 kPa to ensure static slope stability prior to the application of the input ground motion. We also applied an analogous concept to the selection of material properties for frictionless soils alongside the two relationships (Sun *et al.* 2012, Terzaghi and Peck 1967). As a result, this study considers six slope models (three values of β × two soil types) for the nonlinear time history analyses of the slopes. Depending on the V_S values given to each slope model, we applied four types of input ground motions (M2, M3, M4, and M5) to the six slope models. The slope models of the dense frictional and stiff frictionless soils (V_S = 300 m/s) are only compatible with two types of input ground motions, namely, M2 ($V_S \geq$ 260 m/s) and M4 ($V_S \geq$ 180 m/s), whereas the slope models with V_S = 150 m/s for the loose frictional and soft frictionless soils are compatible with all types of input ground motions, namely, M2, M3 (V_S < 260 m/s), M4, and M5 (V_S < 180 m/s).

PLAXIS^{2D} is used to perform nonlinear time-history analyses of the slopes. PLAXIS^{2D} contains a Hardening Soil Model with small-strain stiffness (HSsmall) that describes the nonlinear constitutive laws associated with the hysteric energy dissipation of soils under cyclic loading. The HSsmall model parameters are divided in terms of stiffness and strength. The stiffness parameters include G_0^{ref}; E_{50}^{ref}; E_{oed}^{ref}; E_{ur}^{ref}; υ_{ur}; m; and $\gamma_{0.7}$ (G_0^{ref} is the small-strain shear modulus at a reference pressure; E_{50}^{ref} is the secant stiffness in standard drained triaxial test at a reference pressure; E_{ur}^{ref} is the unloading/reloading stiffness from drained triaxial test at a reference pressure; υ_{ur} is the Poisson's ratio for unloading-reloading; m is the power for stress-level dependency of stiffness; and $\gamma_{0.7}$ is the threshold shear strain at which $G_S = 0.722G_0$. G_S and G_0 are secant and small-strain shear moduli). The G_0^{ref}, E_{50}^{ref}, E_0^{ref}, and E_{oed}^{ref} are assumed as $G_0^{ref} = \rho \cdot V_S^2$, $E_{50}^{ref} = E_{ur}^{ref}/3$, $E_0^{ref} = 10 \cdot E_{ur}^{ref}$, and $E_{oed}^{ref} = E_{50}^{ref}$. The $E_{oed}^{ref} = E_{50}^{ref}$, υ_{ur} = 0.2, and m = 0.5 are used, which are default in this material model.

The superscript of each parameter, ref, refers to a reference pressure which is assumed to be 1 atm. The strength parameters are c, ϕ, and S_u that are listed in Table 3. We computed yield acceleration (ky) values for the 12 slope models using Slide 2 software (Rocscience, 2022) and the resulting values are listed in Table 3. Table 4 listed seven required input parameters for HSsmall model in PLAXIS^{2D}. The $\gamma_{0.7}$ values of each layer obtained from Darendeli (2001) for each layer as shown in Fig. 3. We used Rayleigh damping to model small-strain damping. We adopted D_{min} computed from Darendeli (2001) curves for two soil types as the Rayleigh damping ratio (a damping ratio of 0.7–1.4% and 0.8–1.5% for the frictional and frictionless soils, respectively). The Rayleigh damping formulation requires specifying the two frequencies. We adopted the fundamental frequency of the system ($f_1 = V_S/(4\times H)$ where H = 20 m, which is the entire height of the slope model) for the first frequency and $5\times f_1$ based on Kwok *et al.* (2007) for the second frequency (f_2).

3.1.3 Boundary condition

For nonlinear time history analysis of slopes using PLAXIS^{2D}, we selected the suitable boundary condition with the requirements of slope models. The free-field with the requirements of slope models. The free-field (Cundall *et al.* 1980) and compliant base (Lysmer and Kuhlemeyer 1969) boundary conditions were applied at the lateral sides and bottom of the slope model, respectively, in the nonlinear time history analyses of slopes to minimize the artificially reflected waves at each boundary (Fotopoulou and Pitilakis 2013, Fotopoulou and Pitilakis 2015, Morales-Esteban *et al.* 2015). The acceleration time series of the prepared input motion sets is integrated with the velocity time series to calculate the time series of the shear stresses as follows

Table 4 Required input parameters for HSsmall model in PLAXIS[2D]

Layer	V_S (m/s)	$E_0^{ref} = E_{oed}^{ref}$ (kN/m²)	E_{ur}^{ref} (kN/m²)	G_0^{ref} (kN/m²)	$\gamma_{0.7}$		m	υ
					Frictional soil	Frictionless soil		
1	150	2324	6972	43578	8.03E-05	0.000156	0.5	0.2
2					0.000119	0.000227		
3					0.00015	0.000265		
4					0.000174	0.000297		
1	300	9786	29358	183486	8.25E-05	0.000159	0.5	0.2
2					0.000125	0.00023		
3					0.000156	0.000269		
4					0.00018	0.000301		

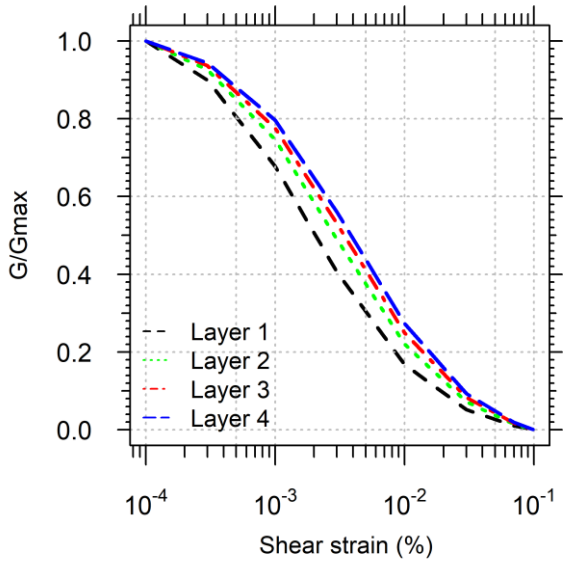

(a) Shear modulus reduction for the frictional soil

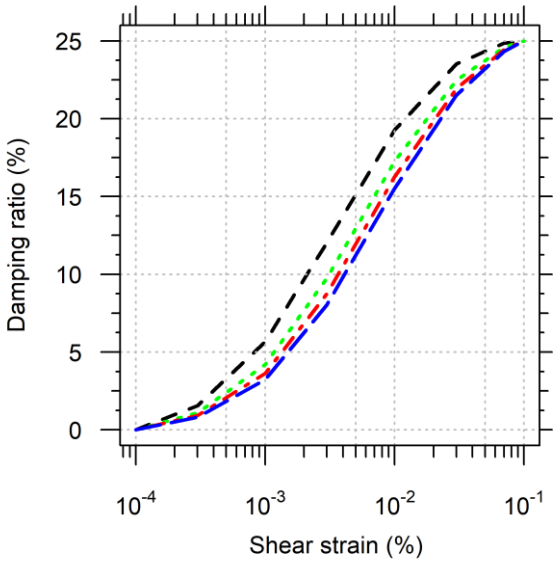

(b) Damping ratio for the frictional soil

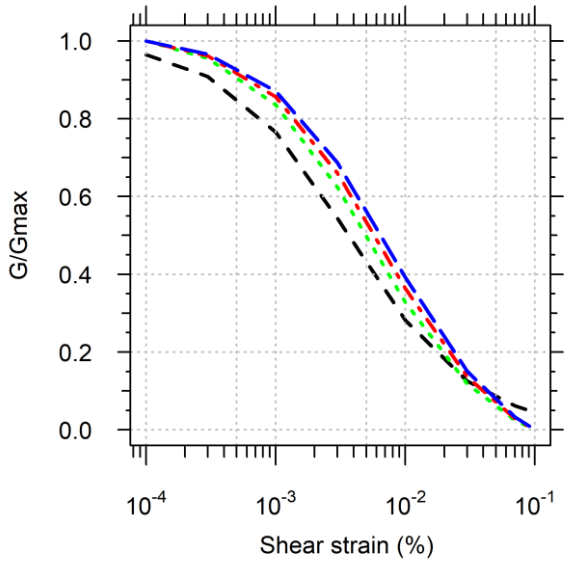

(c) Shear modulus reduction for the frictionless soil

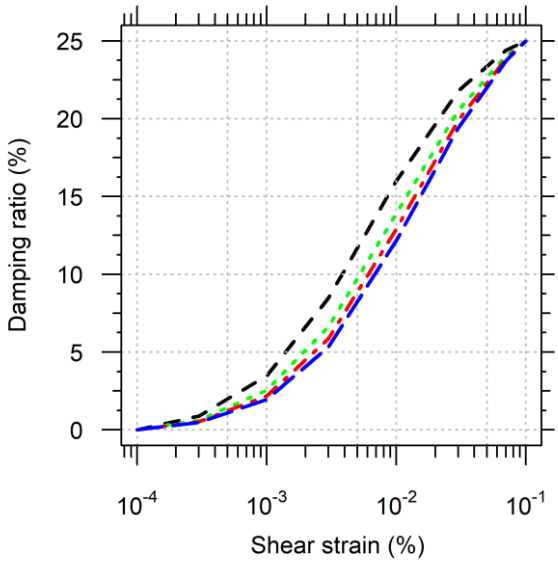

(d) Damping ratio for the frictional soil

Fig. 3 Nonlinear soil curves including shear modulus reduction (G/G_{max}) and damping ratio curves applied to the four sublayers of the soil slope models

$$\tau(t) = \rho_{base} \times V_{S,base} \times \dot{u}_h(t) \quad (1)$$

where $\tau(t)$ is the shear stress time history at the base of the slope model; ρ_{base} is the density of the base of the slope model (1,937 and 2,039 kg/m^3 for the loose frictional and soft frictionless soils and for the dense frictional and stiff frictionless soils, respectively); $V_{S,base}$ is the shear wave velocity of the base of the slope model (150 m/s and 300 m/s for the loose frictional and soft frictionless soils and for the dense frictional and stiff frictionless soils, respectively); and $\dot{u}_h(t)$ is the velocity time series of the input motion.

We applied the acceleration time series of the compiled input ground motions to the bottom of the slope models. We utilized a triangular element consisting of 15 nodes that employs fourth-order displacement interpolation and 12 Gauss points for numerical integration, ensuring precise stress results. The maximum element size in average ($l_{max,avg}$) was determined from the recommendation of Lysmer and Kuhlemeyer (1969) as follows: $l_{max,avg} \leq \lambda/8 = V_{S,min}/8 \cdot f_{max}$, where λ is the minimum wavelength from the input ground motion, $V_{S,min}$ is the smallest V_S in the finite element model, and f_{max} is the highest frequency of the input ground motion. In our analysis, we ensured that the element size was smaller than 1.875 m, which was computed based on the values of $V_{S,min}$ and f_{max} with 150 m/s and 10 Hz, respectively.

3.2 Model verification

We verified our modeling method on the nonlinear time history analysis of slopes by comparing the horizontal displacement of our modeling with that of the previous studies on the nonlinear time history analysis of slopes using PLAXIS^{2D} and FLAC^{2D} (Latha and Garaga 2010, Özmen 2019, Zhang *et al.* 2012). We modeled the three slopes in PLAXIS^{2D} that were created in the previous studies (slope geometries, material properties of the soils, and the free-field and compliant base boundary conditions) and applied the same input ground motions that were used in the previous studies to each slope model. The horizontal displacements computed in this study agree well with those obtained in the previous studies over the entire duration, as shown in Fig. 4. Note that the difference in the displacement value at the end of the input ground motion between the present and earlier studies is less than 4%. Additionally, we calculated R^2 values for the differences of the displacement time series between our results and the previous studies. The R^2 values are 0.97, 0.88, and 0.98 for the analyses of Özmen (2019), Latha and Garaga (2010), and Zhang *et al.* (2012), respectively. These values are approximate to 1.0, indicating that our modeling of a slope is reliable.

3.3 Nonlinear time history analyses

We performed the nonlinear time history analyses of the six slope models (three β × two soil types) combined with the input ground motion type [M2, M3, M4, and M5; each of which has 70 records (= five PGA levels × 14 records)]. The analyses with the loose frictional and soft frictionless soil slopes produced 1,680 values for D_{max} (two soil types × three β × four types of input ground motions × 70 records), and the analyses with the dense frictional and stiff frictionless soil slopes resulted in 840 values for D_{max} (two soil types × three β × two types of input ground motions × 70 records). All the analyses lead to 2,520 values for D_{max}. Additionally, we performed the same number of analyses (= 2,520) with the input ground motions scaled with respect to the five I_A levels (= 0.5, 1.0, 5.0, 10.0, and 15.0 m/s).

Fig. 5 shows the contour plots of the resultant displacement at the end of the earthquake loading (the 2016 M5.8 Gyeongju earthquake) for the loose frictional soil slope model (V_S = 150 m/s and β = 30°) subjected to the four types of input ground motions (M2, M3, M4, and M5) for a PGA of 0.5 g. The M2 type (shallow/stiff site condition) results in smaller displacements than the M3 type (shallow/soft), because the ground motions of the stiff site are generally less amplified than those at the soft site for a given site depth [observe that the analogous trend is observed when comparing the displacements caused by the M4 type (deep/stiff) with those caused by the M5 type deep/soft)]. The displacements caused by M4 (deep/stiff) are greater than those caused by M2 (shallow/stiff), as the ground motions at the deep site are more amplified than those at the shallow site for the same site stiffness [see that the displacements caused by M5 (deep/soft) are greater than those caused by M3 (shallow/soft)].

Fig. 6 shows a plot of D_{max} versus PGA for three different slope models (three values of β) and a V_S of 150 m/s that are subjected to the four types of input ground motions, namely, M2, M3, M4, and M5. As observed in the results of the displacement contour, the ground motion types representing shallow site conditions (M2 or M3) produced smaller D_{max} than those representing deep site conditions (M4 or M5) for the same stiffness description. For example, D_{max} values for M2, M3, M4, and M5 for β = 30° are 0.02 m, 0.036 m, 0.023 m, and 0.048 m, respectively, at a PGA of 0.5 g for the 2016 **M**5.8 Gyeongju earthquake. In addition, the ground motion types with stiff site conditions (M2 and M4) lead to smaller D_{max} than those with soft site conditions (M3 or M5) for the same depth description. These trends for the three slope models with V_S of 150 m/s are also observed with a V_S of 300 m/s, the results (D_{max} vs. PGA) of which are shown in Fig. A1 in the Appendix A. The D_{max} values for M2 type are smaller than those for M4 type (observe that M2 and M4 have the same stiffness description). Previous studies have commonly used PGA as a reference ground motion intensity measure (Latha and Garaga 2010; Özmen 2019, Rathje and Antonakos 2011, Saygili *et al.* 2008, Seo *et al.* 2022) for evaluating the correlation between the demand parameter and the ground motion intensity measure. Thus, we selected PGA as the reference measure. In addition, we explored the correlation between D_{max} and other ground intensity measures. In addition to PGA, we considered other GMPs such as PGV, peak ground displacement (PGD), cumulative absolute velocity (CAV), I_A, $D_{5\text{-}95}$, and T_m. We also calculated the Pearson correlation coefficient (r) to evaluate the correlation between D_{max} and these GMPs. Figs. 7 and

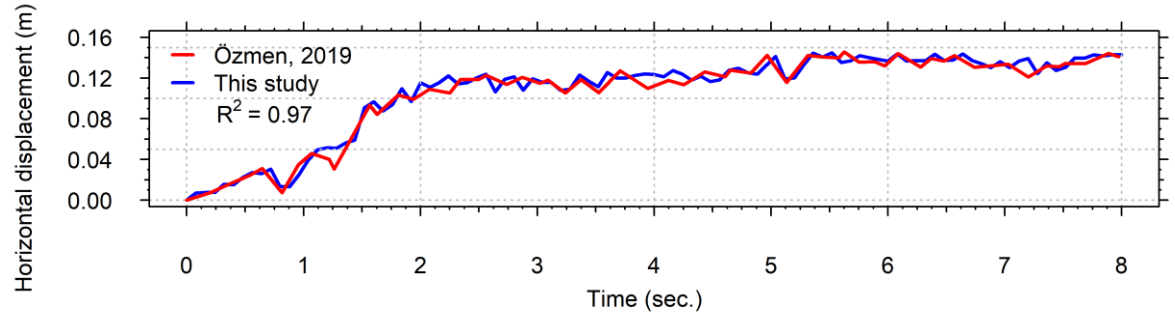

(a) Özmen (2019)

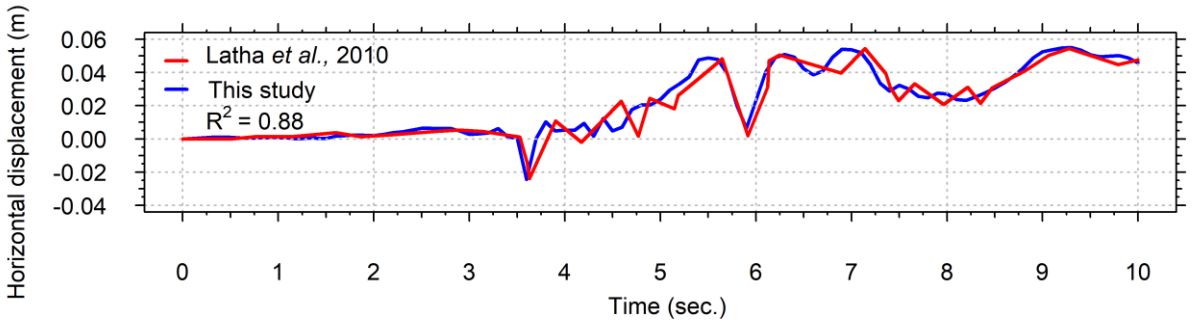

(b) Latha and Garaga (2010)

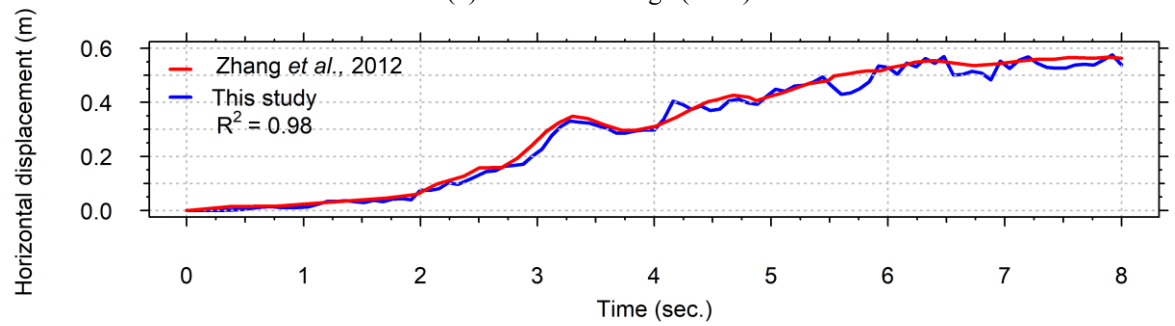

(c) Zhang *et al.* (2012)

Fig. 4 Comparison of horizontal displacement time series between this study and the previous studies

8 show the variation of D_{max}, for the slope model (β = 30° and V_S = 150 m/s), with these six parameters for the frictional and frictionless soil slopes, respectively. It is observed that PGV and I_A have strong correlations with D_{max}. The r values computed for the frictional soil slope are the highest for PGV and I_A (0.78). For frictionless soil slopes, the r value for I_A is the highest (0.77) and the second highest for PGV (0.76). On the other hand, T_m and $D_{S5\text{-}95}$ show weak correlations with D_{max}; the r values of T_m and $D_{S5\text{-}95}$ are 0.54 and 0.38, respectively, for the frictional and 0.56 and 0.37, respectively, for the frictionless soil slopes. Based on these correlations, we selected I_A as an additional parameter for developing fragility surfaces. Furthermore, this ground motion parameter has been considered as the most efficient for seismic slope stability (Campbell and Bozorgnia 2012, Jibson 2007). Figs. A2 and A3 in the Appendix A illustrate the relationship between D_{max} and I_A for the three slope models (three values of β), for V_S = 150 m/s and 300 m/s, respectively, both of which were subjected to the input ground motion types listed in Table 3.

4. Seismic fragility analyses

The seismic fragility of the slopes was evaluated using the PSDM. We developed the seismic fragility curves and surfaces as functions of one GMP and two GMPs, respectively. The following two subsections present the methodology and results for the seismic fragility curves and surfaces.

4.1 Methodology

Developing the fragility curves requires that the limit states associated with specific threshold values of D_{max} be defined. The California Geological Survey (Perez *et al.* 2012) suggested limit states based on three earthquake-induced slope displacements (5, 15, and 30 cm). Using these three limit states, we defined four damage states (minor: D_S < 5 cm; moderate: 5 cm < D_S < 15 cm; extensive: 15 cm < D_S < 30 cm; and collapse: D_S > 30 cm).

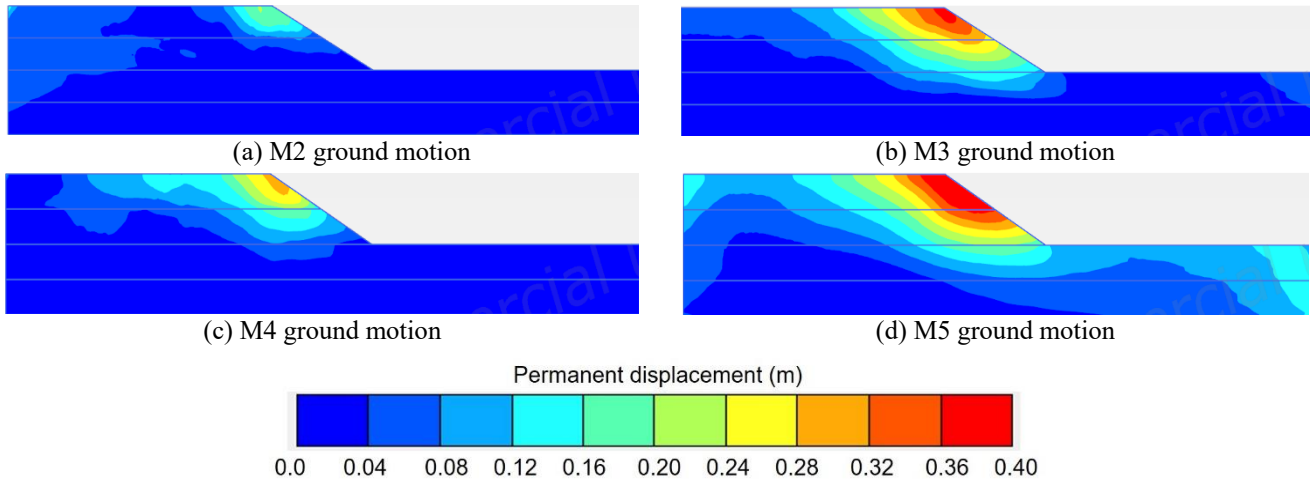

(a) M2 ground motion (b) M3 ground motion

(c) M4 ground motion (d) M5 ground motion

Fig. 5 Permanent displacements (unit: m) computed for models of the frictional soil slopes with V_S of 150 m/s and β of 30° subjected to input ground motions of which PGAs are 0.5 g for the 2016 **M**5.5 Gyeongju earthquake

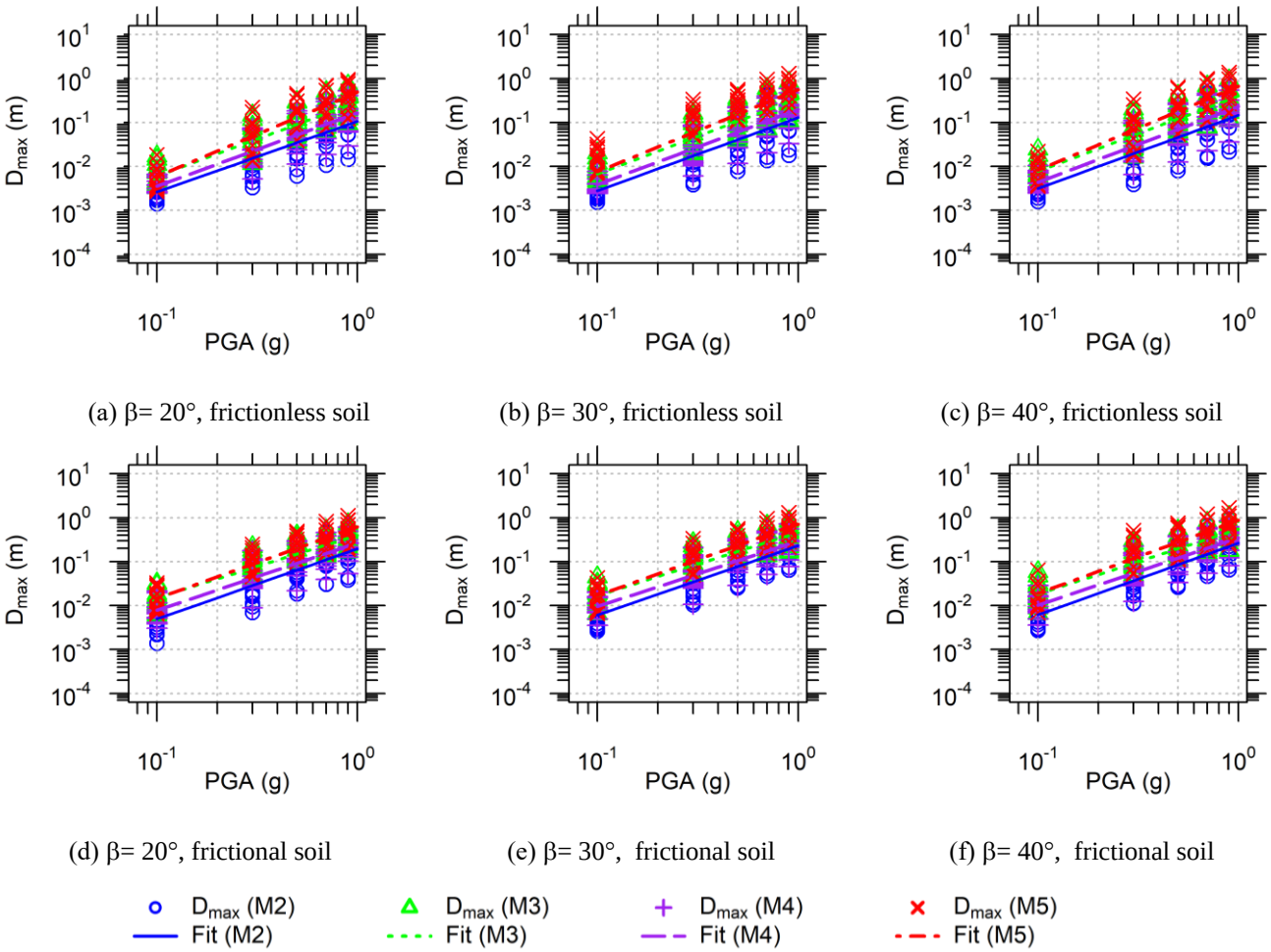

(a) β= 20°, frictionless soil (b) β= 30°, frictionless soil (c) β= 40°, frictionless soil

(d) β= 20°, frictional soil (e) β= 30°, frictional soil (f) β= 40°, frictional soil

Fig. 6 Maximum permanent slope displacements (D_{max}) versus PGA for the four types of input ground motions for frictionless soil slope models with V_S of 150 m/s

Padgett and DesRoches (2008) expressed the probability of a seismic demand exceeding a certain limit state for a given GMP (P_f) that represents a seismic fragility curve as follows

$$P_f = P[D \geq C|GMP] \quad (2)$$

where $P[\cdot]$ is the probability of exceeding the limit state of D; D is the seismic demand (the D_{max} computed from the

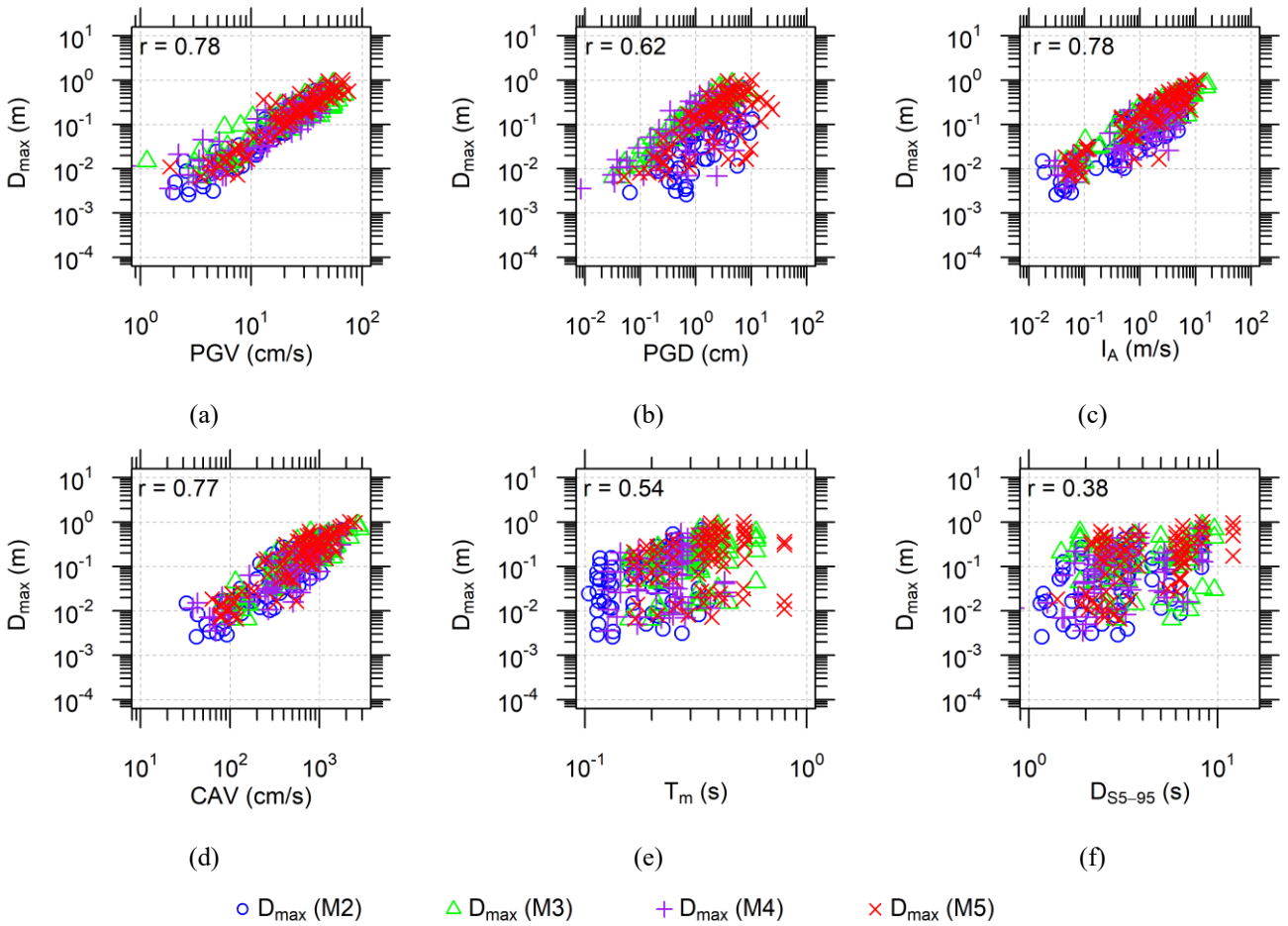

Fig. 7 D_{max} for the six ground motion parameters: (a) PGV; (b) PGD; (c) I_A; (d) CAV; (e) T_m; and (f) $D_{5\text{-}95}$ for the frictional soil slope model with β of 30° and V_S of 150 m/s. The Pearson correlation coefficient (r) for each ground motion parameter is presented

nonlinear time history analyses in Section 3.3); and C is the capacity of the slope (the threshold D_{max} values of 5, 15, and 30 cm). The PSDM represents the relationship between D_{max} and GMPs (PGA or I_A), which can be expressed as follows

$$\ln(D_{max}) = \ln(a) + b \times \ln(GMP) \tag{3}$$

where a and b are the coefficients derived from the regression analysis. It is assumed that D_{max} and GMP are lognormally distributed (Cornell *et al.* 2002, Hariri-Ardebili and Saouma 2016, Padgett and DesRoches 2008). We estimated a and b for the 36 cases of numerical simulations [three β × (two values of V_S × two soil types × two types of input ground motions (M2 and M4) + one value of V_S × two soil types × two types of input ground motions (M3 and M5))] using Eq. (3) with GMP = PGA, and summarized the derived values of a and b for each case as shown in Table 5.

The fitted lines of D_{max} against PGA are shown in Fig. 6 and Fig. A1 in Appendix A for the three slope models, for V_S of 150 m/s and 300 m/s, respectively. Figs. A2 and A3 in Appendix A display the fitted lines of D_{max} versus I_A for the three slope models for V_S of 150 m/s and 300 m/s, respectively.

We computed the probability of D_{max} exceeding the limit state as follows

$$P[D \geq C|GMP] = \Phi\left(\frac{\ln(D) - \ln(C)}{\sqrt{\beta_{D|IM}^2 + \beta_C^2 + \beta_M^2}}\right) \tag{4}$$

where $\Phi(\cdot)$ is the standard normal cumulative distribution function; D is the seismic demand [D_{max} derived from Eq. (3)]; C is the threshold value of the limit state; $\beta_{D|IM}$ is the logarithmic standard deviation of the seismic demand; β_C is the logarithmic standard deviation accounting for the uncertainty in the limit state; and β_M is the logarithmic standard deviation describing the modeling uncertainty. We considered β_C and β_M to be 0.3 and 0.4, respectively, as suggested by Wen *et al.* (2004) and HAZUS-MH (2003).

Jafarian and Miraei (2019) suggested $\beta_{D|IM}$ as follows

$$\beta_{D|IM} = \sqrt{\frac{\sum_{i=1}^{N}[\ln(d_i) - \ln(a \times GMP^b)]^2}{N-2}} \tag{5}$$

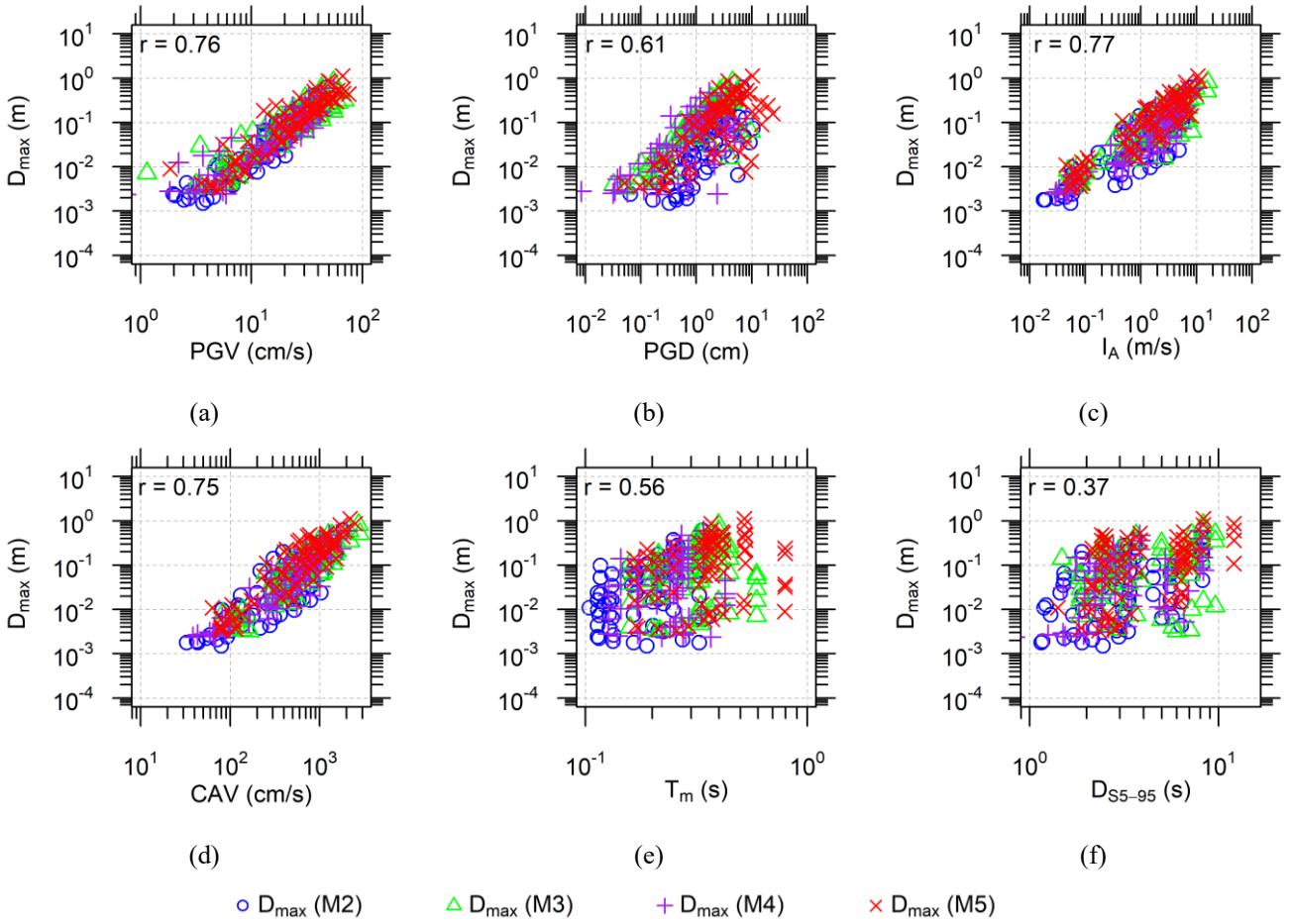

Fig. 8 D_{max} against the six ground motion parameters: (a) PGV, (b) PGD, (c) I_A, (d) CAV, (e) T_m and (f) $D_{5\text{-}95}$ for the frictionless soil slope model with β of 30º and V_S of 150 m/s. The Pearson correlation coefficient (r) for each parameter is presented

where N is the total number of the ground motions (N=70, that is, 14 ground motions calculated for each site condition × five levels of GMPs) and d_i are the values of D_{max} computed for each ground motion. As listed in Table 5, $\beta_{D|IM}$ for the PGA-based PSDM ranges from 0.59 to 0.90, which is slightly lower than that for the I_A-based PSDM (0.59 to 0.92).

4.2 Fragility curves and surfaces

Fig. 9 shows the effect of soil type [frictionless (S_u = 48 kPa) and frictional (c = 10 kPa and ϕ = 30°) soils] applied to the slope model with β of 30° and V_S of 150 m/s (this V_S value corresponds to the loose and soft states of soils) on the fragility curves for the three limit states across the four types of input ground motions. We observed from Fig. 9 that the probabilities of exceeding the three limit states for the soft frictionless soil slope are lower than those for the loose frictional soil slope across the four types of input ground motions. For instance, the probabilities of exceeding the moderate state for the frictionless soil slope are 0.10, 0.34, 0.16, and 0.51 for M2, M3, M4, and M5 types, respectively, at a PGA of 0.5 g. On the other hand, the probabilities for the frictional soil slope are 0.23, 0.56, 0.33, and 0.72, respectively. Note that these results are specific to the slope models utilized in this study and may not hold true for other cases of frictional and frictionless soil slopes. Figs. B1 and B2 in Appendix B. indicate similar trends for the probabilities of exceeding the three limit states, for the frictionless (S_u = 48 kPa) and frictional (c = 10 kPa and ϕ = 30°) soil slopes, respectively; the values of β are 20° and 40° for the same V_S (= 150 m/s), across the four types of input ground motions.

Fig. 10 illustrates the influence of β on the fragility curves for the loose frictional soil slope (V_S = 150 m/s). The increase in β results in higher probabilities for the four types of input ground motions and the three limit states. For M2 with a PGA of 0.5 g, the probabilities of exceeding the three limit states are 0.61 (minor), 0.18 (moderate), and 0.05 (extensive) for a slope with β of 20°, whereas for a slope with β of 30° these values are higher, at 0.69 (minor), 0.23 (moderate), and 0.07 (extensive). A similar trend appeared for the soft frictionless soil slope (V_S = 150 m/s), as shown in Fig. B3 in Appendix B.

Fig. 11 and Fig. B4 in Appendix B illustrate the effect of the input ground motion type on the fragility curves for

Table 5 Regression coefficients of PSDMs and dispersion terms for D_{max} against the two GMPs (PGA and I_A) for the 36 cases

Case of numerical simulation				PGA-based PSDM			I_A-based PSDM		
β (°)	Ground motion	Soil type	V_S (m/s)	a	b	$\beta_{D\|IM}$	a	b	$\beta_{D\|IM}$
20	M2	Dense frictional soils	300	0.08	1.75	0.85	0.002	1.64	0.85
		Loose frictional soils	150	0.20	1.60	0.90	0.003	1.49	0.90
		Stiff frictionless soils	300	0.04	1.64	0.78	0.001	1.53	0.78
		Soft frictionless soils	150	0.10	1.58	0.92	0.005	1.53	0.92
30	M2	Dense frictional soils	300	0.10	1.29	0.59	0.005	1.34	0.59
		Loose frictional soils	150	0.23	1.58	0.87	0.004	1.53	0.87
		Stiff frictionless soils	300	0.04	1.62	0.74	0.001	1.50	0.74
		Soft frictionless soils	150	0.13	1.66	0.91	0.006	1.50	0.91
40	M2	Dense frictional soils	300	0.11	1.20	0.61	0.007	1.26	0.61
		Loose frictional soils	150	0.26	1.63	0.90	0.005	1.57	0.90
		Stiff frictionless soils	300	0.04	1.60	0.76	0.002	1.50	0.76
		Soft frictionless soils	150	0.15	1.66	0.91	0.007	1.52	0.91
20	M3	Loose frictional soils	150	0.40	1.43	0.64	0.025	1.49	0.64
		Soft frictionless soils	150	0.29	1.69	0.80	0.048	1.30	0.80
30	M3	Loose frictional soils	150	0.46	1.43	0.69	0.029	1.49	0.69
		Soft frictionless soils	150	0.35	1.72	0.75	0.052	1.34	0.75
40	M3	Loose frictional soils	150	0.55	1.48	0.73	0.032	1.48	0.73
		Soft frictionless soils	150	0.40	1.71	0.76	0.062	1.34	0.76
20	M4	Dense frictional soils	300	0.15	1.86	0.63	0.006	1.58	0.63
		Loose frictional soils	150	0.27	1.53	0.68	0.008	1.52	0.68
		Stiff frictionless soils	300	0.07	1.86	0.56	0.003	1.66	0.56
		Soft frictionless soils	150	0.17	1.67	0.70	0.014	1.40	0.7
30	M4	Dense frictional soils	300	0.16	1.37	0.58	0.013	1.35	0.58
		Loose frictional soils	150	0.29	1.49	0.67	0.009	1.55	0.67
		Stiff frictionless soils	300	0.07	1.84	0.57	0.003	1.64	0.57
		Soft frictionless soils	150	0.20	1.71	0.70	0.016	1.41	0.70
40	M4	Dense frictional soils	300	0.17	1.30	0.59	0.016	1.31	0.59
		Loose frictional soils	150	0.35	1.54	0.67	0.009	1.57	0.67
		Stiff frictionless soils	300	0.08	1.82	0.60	0.003	1.63	0.60
		Soft frictionless soils	150	0.23	1.72	0.72	0.018	1.43	0.72
20	M5	Loose frictional soils	150	0.61	1.60	0.62	0.089	1.34	0.62
		Soft frictionless soils	150	0.49	1.92	0.78	0.150	1.23	0.78
30	M5	Loose frictional soils	150	0.72	1.62	0.65	0.105	1.33	0.65
		Soft frictionless soils	150	0.56	1.87	0.72	0.156	1.28	0.72
40	M5	Loose frictional soils	150	0.88	1.66	0.68	0.119	1.31	0.68
		Soft frictionless soils	150	0.67	1.91	0.73	0.190	1.26	0.73

the frictionless and frictional soil slope models, respectively, with β = 20°, 30°, and 40° and V_S = 150 m/s. For a given depth description (shallow or deep), M2 (or M4) that represents a stiff site condition produced lower probabilities of exceeding each limit state than M3 (or M5) that is representative of a soft site condition. In addition, for a given stiffness description (stiff or soft), M2 (or M3) that represents a shallow site condition resulted in smaller probabilities of exceeding each limit state than M4 (or M5) that is representative of a deep site condition. For example, the probabilities of exceeding the minor limit state with a β of 30° in Fig. 11 are approximately 0.42, 0.81, and 0.58 for M2, M3, and M4, respectively, at a PGA of 0.5 g. The probability for M3 is approximately 1.93 times higher than that for M2, given the same depth description. The probability for M4 is approximately 1.38 times greater than that for M2 for the same stiffness description.

Fig. 12 presents the fragility curves of the stiff frictionless (S_u = 72 kPa) and dense frictional (c = 10 kPa and f = 40°) soil slopes for V_S = 300 m/s and β = 20°, 30°, and 40° across two types of the input ground motions, namely M2 and M4. The probabilities of exceeding each limit state due to M4 are mostly higher than those due to M2 across the three β for a given soil type. For instance, the probabilities of exceeding the minor state for the dense frictional soil slope subjected to M2 at a PGA of 0.7 g are 0.45, 0.60, and 0.66, for β = 20°, 30°, and 40° [Figs. 12(a)-12(c)], respectively. On the other hand, the probabilities of exceeding the minor state in the case of dense frictional soil slopes subjected to M4 motion at a PGA of 0.7 g are 0.70, 0.81, and 0.86 [Figs. 12(d)-12(f)], respectively. In addition,

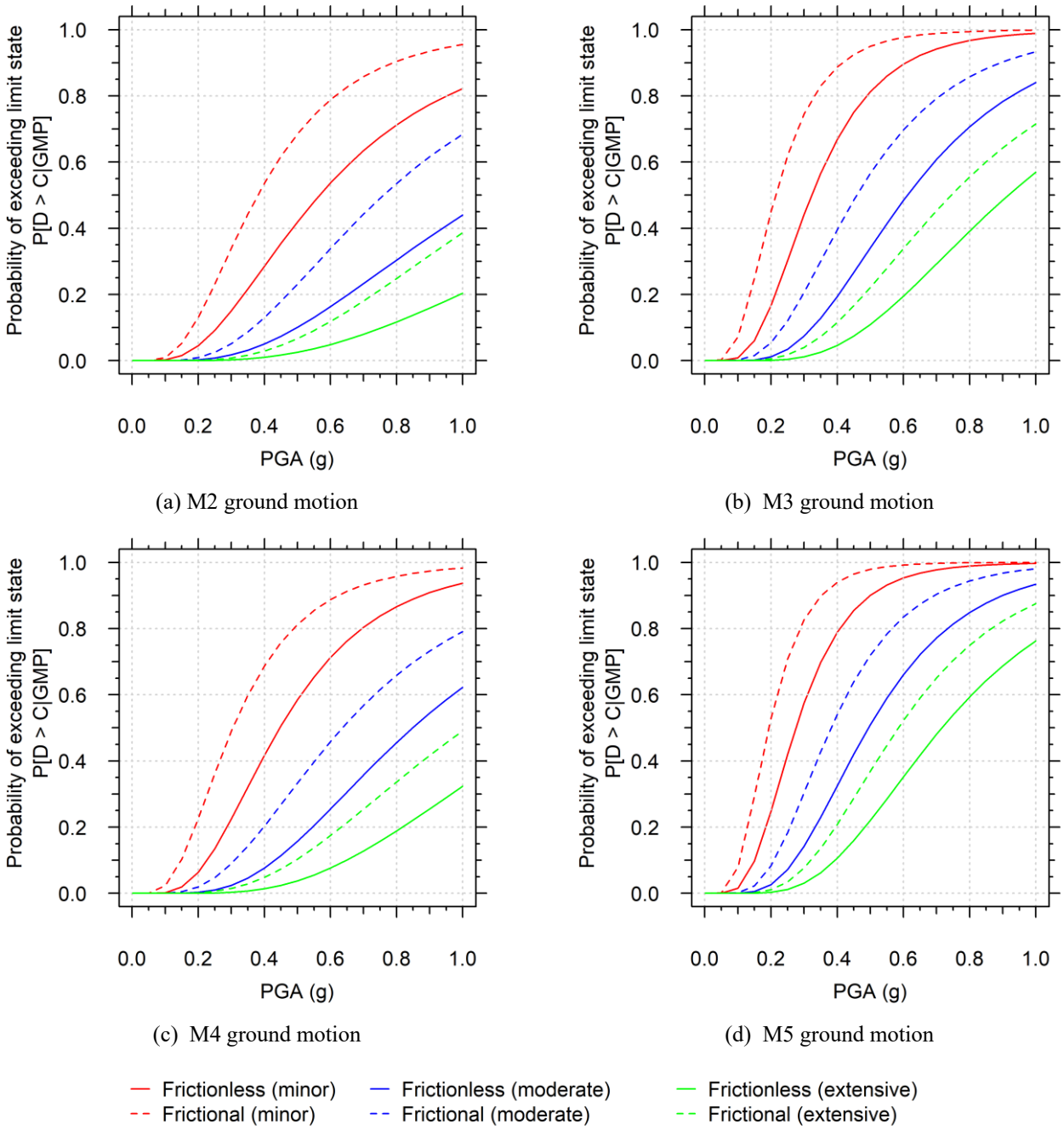

Fig. 9 Seismic fragility curves with respect to PGA for the frictional and frictionless soil slopes with β of 30° and V_S of 150 m/s subjected to the four types of ground motions

The probabilities of exceeding the limit states in the case of stiff frictionless soil slopes are mostly smaller than those for dense frictional ones, across the two types of input ground motions, which is similar to that observed in Fig. 9.

We also developed fragility curves with respect to I_A. Figs. C1 through C3 in Appendix C illustrate the probabilities of exceeding the three limit states for the frictionless and frictional soil slopes and for three values of β (V_S of 150 m/s) across the four types of input ground motions. Fig. C4 in Appendix C shows the probabilities of exceeding the three limit states for the frictionless and frictional soil slopes for three different β values across two types of input ground motions at a V_S of 300 m/s. The trends of the probabilities of limit state exceedance versus I_A for the two V_S are generally analogous to those versus PGA with respect to the influence of β, input ground motion type, and soil type. After examining the Pearson coefficients (r) for the six GMPs (PGV, PGD, I_A, $D_{S5\text{-}S95\%}$, CAV, and T_m), I_A led to the greatest r values across all the slope models considered. In addition, there have been several studies on selecting I_A as an optimal GMP for analyzing the seismic behaviors of structures (Hu and Pang 2023, Travasarou

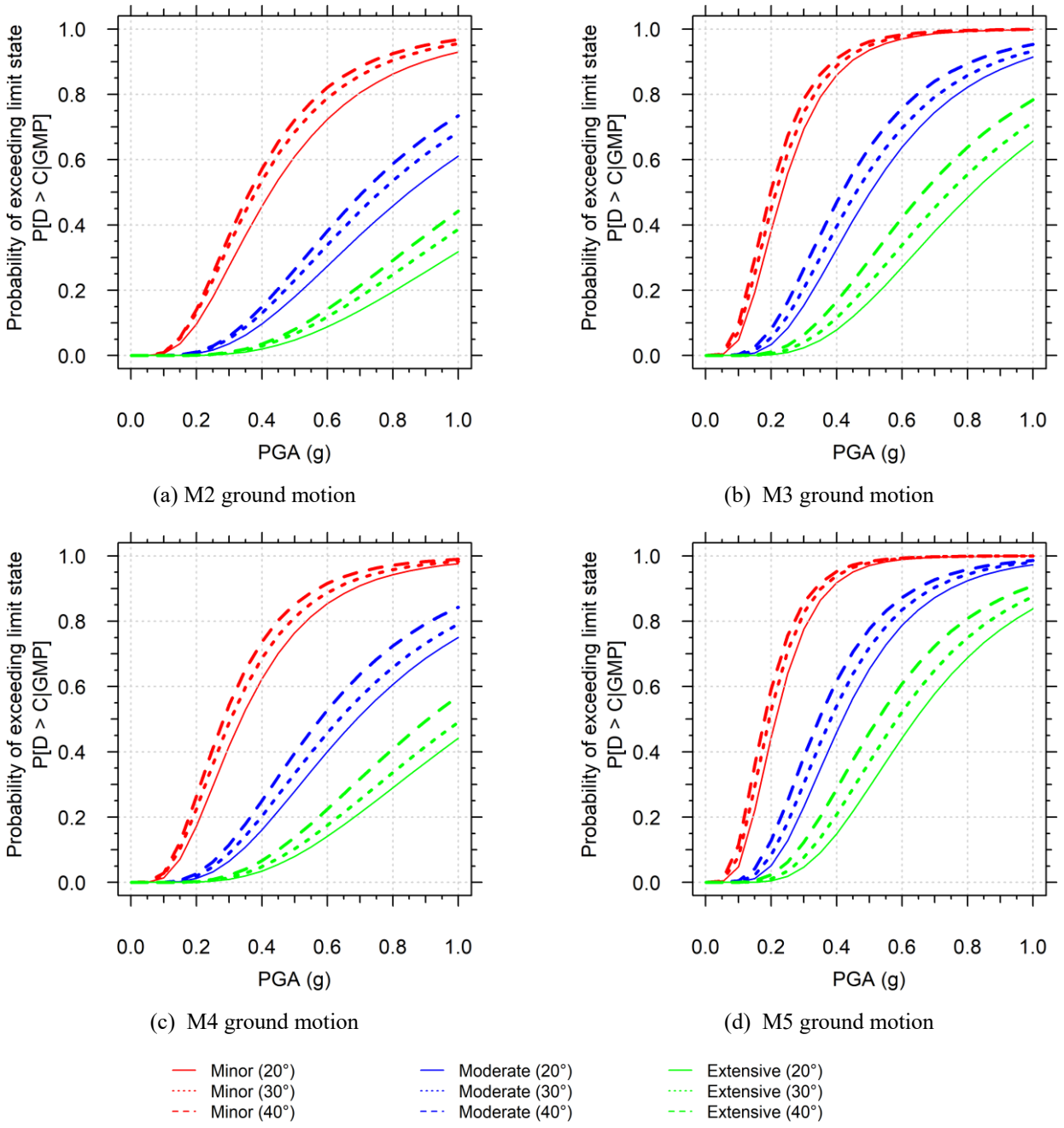

Fig. 10 Seismic fragility curves with respect to PGA for frictional soil slopes with three β (= 20º, 30 º, and 40º) and V_S of 150 m/s subjected to four types of ground motions

and Bray 2003). Thus, we chose I_A as a secondary GMP for investigating the seismic fragility surface of the fill slope. We also developed seismic fragility surfaces to investigate the effects of multiple GMPs on seismic demand (D_{max}). The PSDM for the relationship between D_{max} and two GMPs, namely PGA and I_A, simultaneously, can be expressed as follows

$$\ln(D_{max}) = e_1 + e_2 \times \ln(GMP_1) + e_3 \times \ln(GMP_2) \quad (6)$$

where e_1, e_2, and e_3 are the regression coefficients, and GMP_1 and GMP_2 are PGA and I_A, respectively.

Fig. 13 shows the seismic fragility surfaces for the soft frictionless and loose frictional soil slopes (V_S = 150 m/s) with β = 30° subjected to M2. The probabilities of exceeding the three limit states increase with both PGA and I_A. The fragility surfaces for other V_S and β values and the four types of input ground motions (M2, M3, M4, and M5) are presented in Figs. D1 through D11 in Appendix D, and Figs. E1 through E6 in Appendix E. The probabilities of exceeding the limit state become greater as β increases. The probabilities for the motions for the soft site conditions (M3 or M5) are mostly greater than those for the stiff site conditions (M2 or M4).

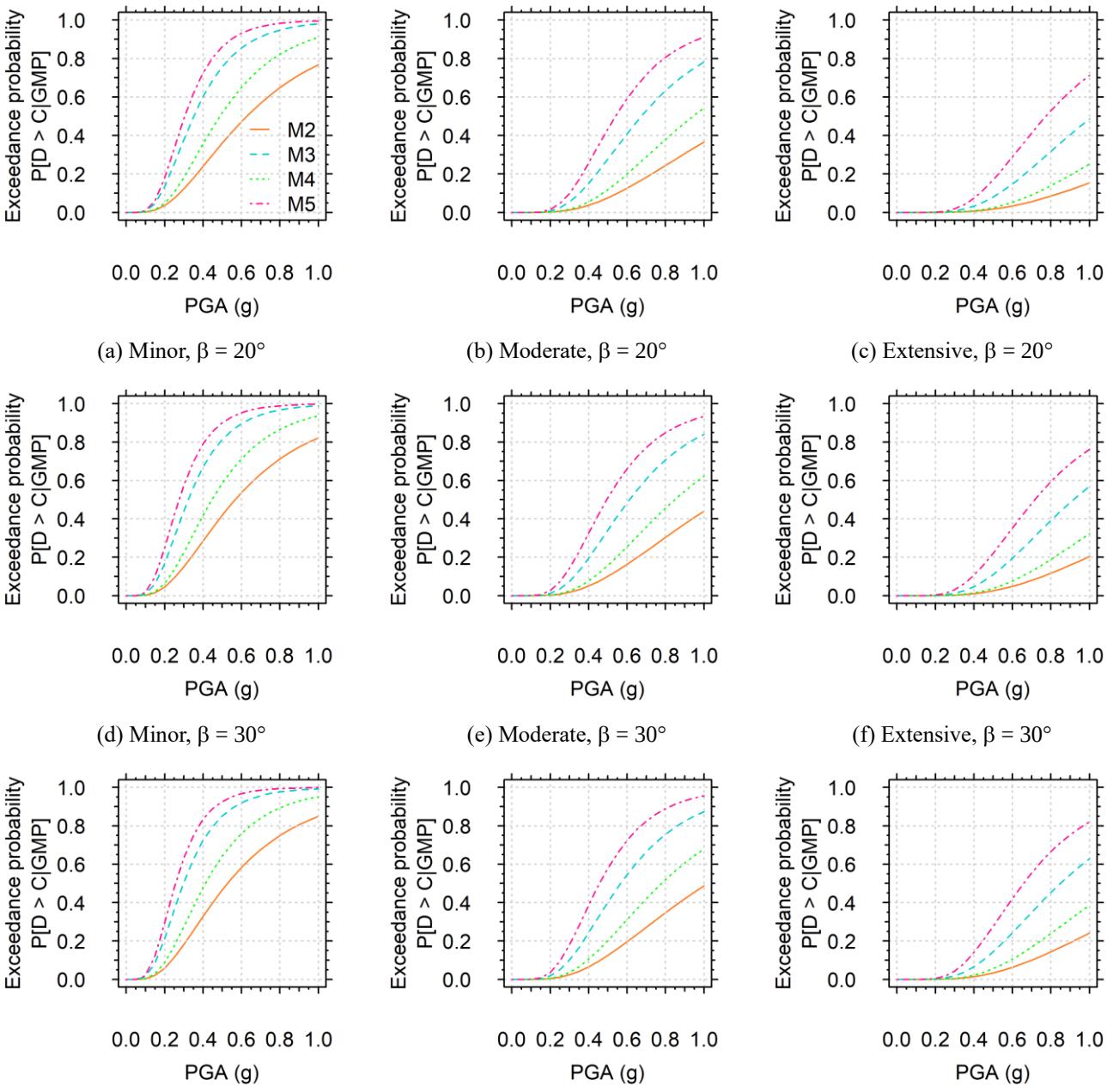

(a) Minor, β = 20° (b) Moderate, β = 20° (c) Extensive, β = 20°

(d) Minor, β = 30° (e) Moderate, β = 30° (f) Extensive, β = 30°

(g) Minor, β = 40° (h) Moderate, β = 40° (i) Extensive, β = 40°

Fig. 11 Seismic fragility curves with respect to PGA for the frictionless soil slopes with V_S of 150 m/s subjected to four types of ground motions (M2, M3, M4, and M5) and for the limit states of minor (left column), moderate (center column), and extensive (right column) for β of 20° (a), (b), and (c); 30° (d), (e), and (f); and 40° (g), (h), and (i)

5. Discussion

We assessed the seismic fragility of the slopes based on two soil types, β values, and input ground motion types, leading to the following observations:

- Effect of soil type on the fragility curve given β and input ground motion type: The probabilities of exceeding the limit states for the frictional soils (loose soils: c = 10 kPa, ϕ = 30°, and V_S = 150 m/s; and dense soils: c = 10 kPa, ϕ = 40°, and V_S = 300 m/s) are mostly greater than those for the frictionless soils (soft soils: S_u = 48 kPa and V_S = 150 m/s; and stiff soils: S_u = 72 kPa and V_S = 300 m/s). Given β = 30°, the probabilities of the loose frictional soil slope for the moderate state are 2.30, 1.65, 2.06, and 1.41 times greater than those of the soft frictionless soil slope for M2, M3, M4, and M5 at a PGA of 0.5 g.
- Effect of β on the fragility curve given soil type and input ground motion type: The probabilities of exceeding the limit states become great as β increases. For M2 at a PGA of 0.5 g, the probabilities of the loose frictional soil slope with β = 30° are 1.13 (minor state), 1.28

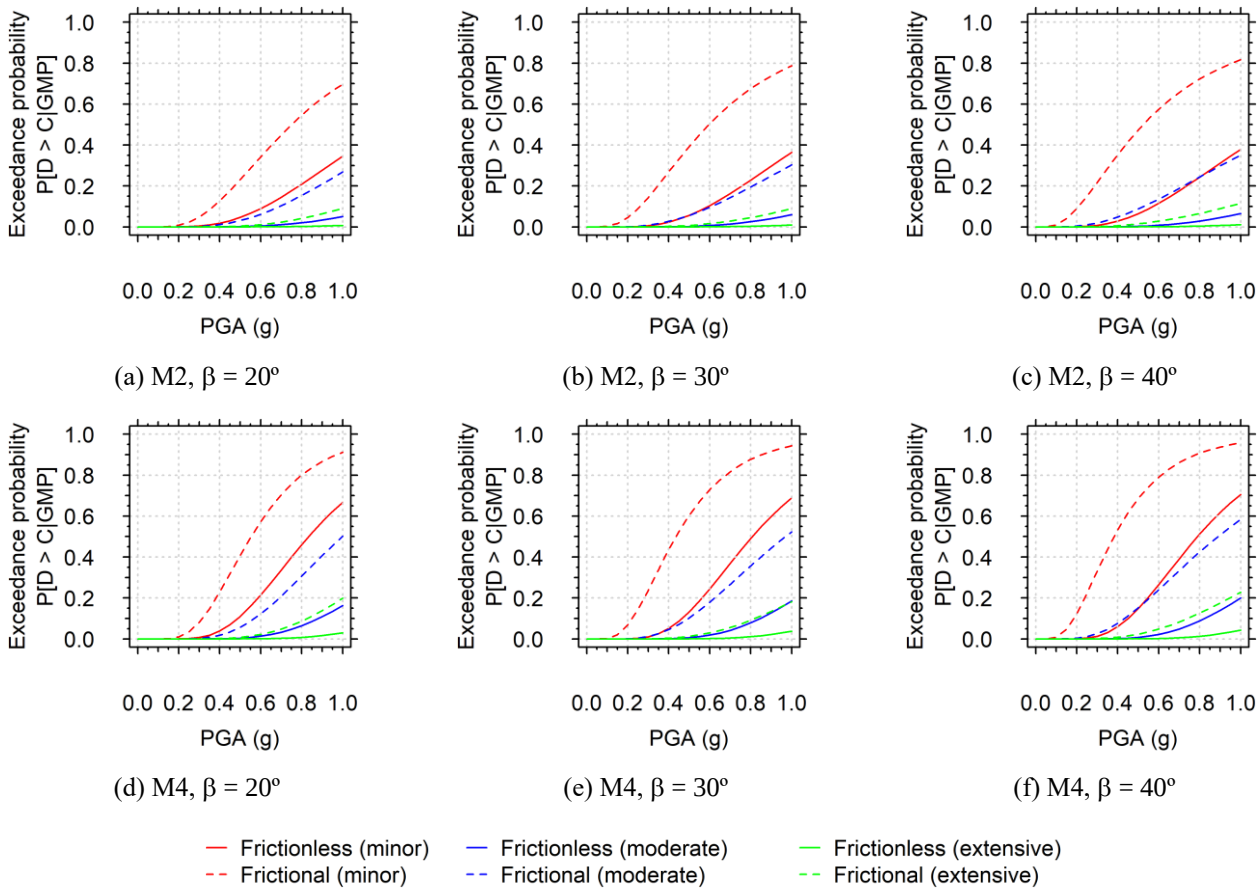

Fig. 12 Seismic fragility curves with respect to PGA for frictionless and frictional soil slopes with V_S of 300 m/s subjected to two types of ground motions M2 and M4.

(moderate state), and 1.40 (extensive state) times higher than those of the loose frictional soil slope with β = 20°.

- Effect of input ground motion type on the fragility curve given soil type and β: The probabilities of exceeding the limit states for the stiff site condition (M2 or M4) are smaller than those for the soft site condition (M3 or M5). For the soft frictionless soil slope of β = 30°, the probability of exceeding the minor limit state for M2 at a PGA of 0.5 g is approximately 0.52 times smaller than that of M3. Additionally, the ground motions for the deep site condition (M4 or M5) produced larger probabilities than those for the shallow site condition (M2 or M3). Given β = 30° and the soft, frictionless soil slope, the probability of exceeding the minor limit state for M2 at a PGA of 0.5 g is approximately 0.72 times lower than that of M4.

6. Conclusions

This study proposed seismic fragility curves and surfaces for fill slopes in South Korea using finite element analysis. We considered three slope geometries with varying β (20°, 30°, and 40°), each having the H_{slope} (10 m) consisting of two soil types (frictional and frictionless) associated with two states of soil (loose and dense for the frictional soils; soft and stiff for the frictionless soils). The input motions were computed for the four site conditions in South Korea (i.e., M2, M3, M4, and M5). The results presented that the type of soil, slope angle, and input ground motion significantly affected the probabilities of the exceeding limit states which is consistent with previous studies. The findings from this study might inform regional authorities and engineers in South Korea of the seismic fragility assessment for road systems and promote strategies to enhance community resilience during earthquakes.

The limitations of our study are that we only considered one criterion to select an optimal GMP for developing fragility curves and performed a single slope height of 10 m. In reality, slopes can have various heights that affect slope stability. Future studies could consider multiple criteria to identify an optimal GMP and investigate the effect of slope heights on the seismic slope fragility results.

Acknowledgments

This work was supported by the National Research Foundation of Korea (NRF) grant funded by the Korean

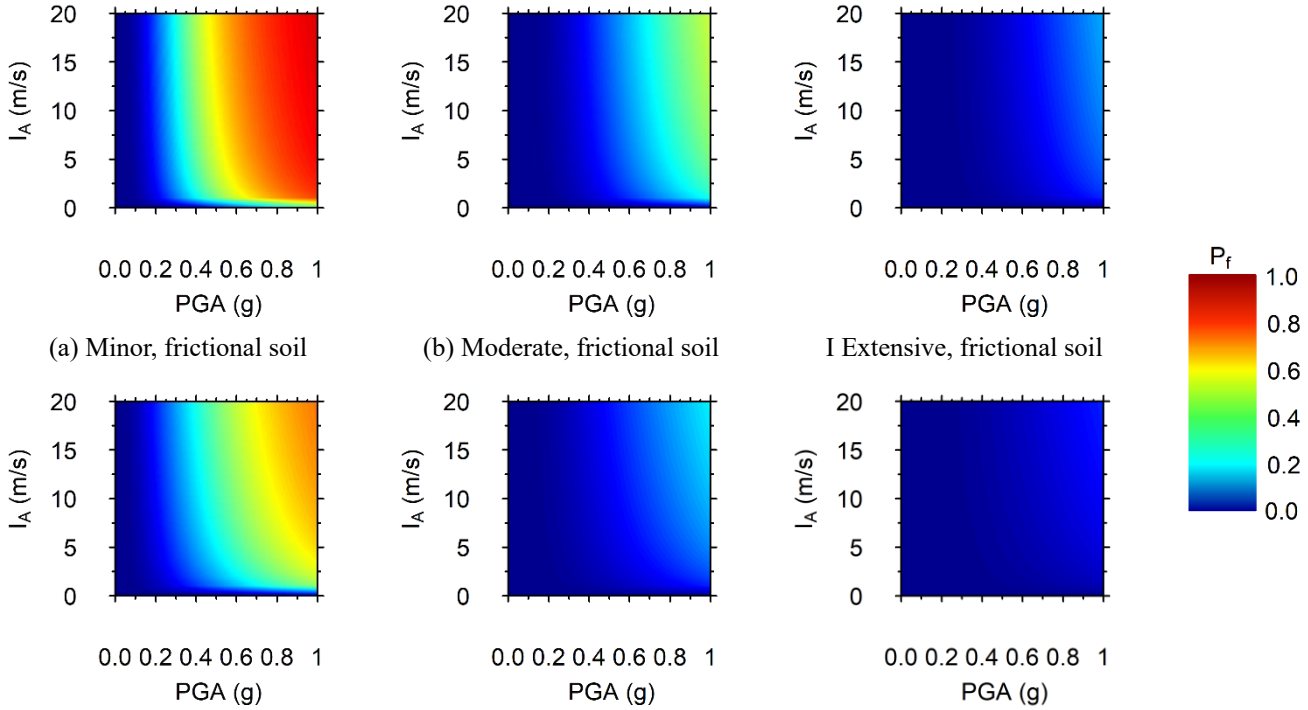

(a) Minor, frictional soil (b) Moderate, frictional soil I Extensive, frictional soil

(d) Minor, frictionless soil (e) Moderate, frictionless soil (f) Extensive, frictionless soil

Fig. 13 Probabilities of exceeding limit state (P_f) with respect to the PGA and I_A for the three limit states the frictional and the frictionless soil slopes with a β of 20° and subjected to M2 motion

Government (MSIT) (NFR--2020R1C1C1013317) and the Korea Meteorological Administration Research and Development Program (PJ0013282021).

References

Anderson, D.G., Martin, G.R., Lam, I.P. and Wang, J.N.J.N.R. (2009), Seismic Analysis and Design of Retaining Walls, Buried Structures, Slopes, and Embankments.

Argyroudis, S., Kaynia, A.M. and Pitilakis, K. (2013), "Development of fragility functions for geotechnical constructions: Application to cantilever retaining walls", *Soil Dyn. Earthq. Eng.*, **50**, 106-116. https://doi.org/10.1016/j.soildyn.2013.02.014

BSSC (2000), The 2000 NEHRP recommended provisions for new buildings and other structures, Part1 (provisions) and Part2 (commentary), 368/369. Washington, D.C: FEMA; 2001.

Campbell, K.W. and Bozorgnia, Y. (2012), "A comparison of ground motion prediction equations for arias intensity and cumulative absolute velocity developed using a consistent database and functional form", *Earthq. Spectra*, **28**(3), 931-941. https://doi.org/10.1193/1.4000067.

CEN (2004), European Committe for Standardization (CEN). EC8 Eurocode 8: design of structures for earthquake resistance. In: Seismic actions and rules for buildings, stage 49 draft. Brussels: Comit´e Europ´een de Normalisation; 2004.

Chen, G., Li, Y., Zhang, Y. and Wu, J. (2012), Earthquake Induced a Chain Disasters, Earthquake Research and Analysis - Statistical Studies, Observations and Planning.

Chiou, J.S., Chiang, C.H., Yang, H.H. and Hsu, S.Y. (2011), "Developing fragility curves for a pile-supported wharf", *Soil Dyn. Earthq. Eng.*, **31**(5-6), 830-840. https://doi.org/10.1016/j.soildyn.2011.01.011.

Cornell, C.A., Jalayer, F., Hamburger, R.O. and Foutch, D.A. (2002), "Probabilistic basis for 2000 SAC federal emergency management agency steel moment frame guidelines", *J. Struct. Eng.*, **128**(4), 526-533. https://doi.org/10.1061/(asce)0733-9445(2002)128:4(526).

Crowley, H., Pinho, R. and Bommer, J.J. (2004), "A probabilistic displacement-based vulnerability assessment procedure for earthquake loss estimation", *Bull. Earthq. Eng.*, **2**, 173-219. https://doi.org/10.1007/s10518-004-2290-8.

Cundall, P., Hansteen, H., Lacasse, S. and Selnes, P. (1980), NESSI: soil structure interaction program for dynamic and statistic problems. Report 51508-9, December, Norwegian Geotechnical Institute.

Darendeli (2001), Development of a new famili of normalized modulus reduction and material damping.

EERI, S.E.R. (2010), The Mw 7.1 Darfield (Canterbury), New Zealand Earthquake of September 4, 2010.

El-Maissi, A.M., Argyroudis, S.A. and Nazri, F.M. (2020), "Seismic vulnerability Assessment methodologies for roadway assets and networks: A state-of-the-art review", *Sustainability*, **13**(1). https://doi.org/10.3390/su13010061.

Erberik, M.A. (2015), Seismic Fragility Analysis, Encyclopedia of Earthquake Engineering, 1-10.

Fotopoulou, S.D. and Pitilakis, K.D. (2013), "Fragility curves for reinforced concrete buildings to seismically triggered slow-moving slides", *Soil Dyn. Earthq. Eng.*, **48**, 143-161. https://doi.org/10.1016/j.soildyn.2013.01.004.

Fotopoulou, S.D. and Pitilakis, K.D. (2015), "Predictive relationships for seismically induced slope displacements using numerical analysis results", *Bull. Earthq. Eng.*, **13**(11), 3207-3238. https://doi.org/10.1007/s10518-015-9768-4.

Hariri-Ardebili, M.A. and Saouma, V.E. (2016), "Probabilistic seismic demand model and optimal intensity measure for concrete dams", *Struct. Saf.*, **59**, 67-85. https://doi.org/10.1016/j.strusafe.2015.12.001

HAZUS-MH (2003), Federal Emergency Management Agency (FEMA). HAZUS-MH MR4 Technical Manual. Natl Inst Build Sci Fed Emerg Manag Agency (NIBS FEMA) 2003.

Hu, H. Huang, Y. and Chen, Z. (2019), "Seismic fragility functions for slope stability analysis with multiple vulnerability states", *Environ. Earth Sci.*, **78**(24), https://doi.org/10.1007/s12665-019-8696-z.

Hu, J. and Pang, L. (2023), "Identifying the optimal intensity measure and key factors of earthquake liquefaction-induced uplift of underground structures", *Bull. Eng. Geol. Environ.*, **82**(1). https://doi.org/10.1007/s10064-022-03057-4.

Jafarian, Y. and Miraei, M. (2019), "Scalar- and vector-valued fragility analyses of gravity quay wall on liquefiable soil: Example of Kobe port", *Int. J. Geomech.*, **19**(5). https://doi.org/10.1061/(asce)gm.1943-5622.0001382.

Jibson, R.W. (2007), "Regression models for estimating coseismic landslide displacement", *Eng. Geol.*, **91**(2-4), 209-218. https://doi.org/10.1016/j.enggeo.2007.01.013.

Kim, D.S., Manandhar, S. and Cho, H.I. (2018), "New site classification system and design response spectra in Korean seismic code", *Earthq. Struct.*, https://doi.org/10.12989/eas.2018.15.1.001.

Kim, J.M. and Sitar, N. (2013), "Probabilistic evaluation of seismically induced permanent deformation of slopes", *Soil Dyn. Earthq. Eng.*, **44**, 67-77. https://doi.org/10.1016/j.soildyn.2012.09.001.

Kwok, A.O.L., Stewart, J.P., Hashash, Y.M.A., Matasović, N., Pyke, R., Wang, Z., Yang, Z.J.J.O.G. and Engineering, G. (2007), "Use of exact solutions of wave propagation problems to guide implementation of nonlinear seismic ground response analysis procedures", *J. Geotech. Geoenviron. Eng.*, **133**(11), 1385-1398. https://doi.org/10.1061/(ASCE)1090-0241(2007)133:11(1385).

Latha, G.M. and Garaga, A. (2010), "Seismic stability analysis of a Himalayan rock slope", *Rock Mech. Rock Eng.*, **43**(6), 831-843. https://doi.org/10.1007/s00603-010-0088-3.

Lee, M.G., Ha, J.G., Cho, H.I., Sun, C.G. and Kim, D.S. (2020), "Improved performance-based seismic coefficient for gravity-type quay walls based on centrifuge test results", *Acta Geotechnica*, **16**(4), 1187-1204. https://doi.org/10.1007/s11440-020-01086-5.

Lysmer, and Kuhlemeyer, (1969), Finite dynamic model for infinit midia, Engineering mechanics division, v. Proceedings of the American Siciety of Civil Engineers.

Maruyama, Y., Yamazaki, F., Mizuno, K., Tsuchiya, Y. and Yogai, H. (2010), "Fragility curves for expressway embankments based on damage datasets after recent earthquakes in Japan", *Soil Dyn. Earthq. Eng.*, **30**(11), 1158-1167. https://doi.org/10.1016/j.soildyn.2010.04.024.

McKenna, G., Argyroudis, S.A., Winter, M.G. and Mitoulis, S.A. (2021), "Multiple hazard fragility analysis for granular highway embankments: Moisture ingress and scour", *Transport. Geotech.*, **26**, 100431. https://doi.org/10.1016/j.trgeo.2020.100431

Morales-Esteban, A., de Justo, J.L., Reyes, J., Miguel Azañón, J., Durand, P. and Martínez-Álvarez, F. (2015), "Stability analysis of a slope subject to real accelerograms by finite elements. application to San Pedro cliff at the Alhambra in Granada", *Soil Dyn. Earthq. Eng.*, **69**, 28-45. https://doi.org/10.1016/j.soildyn.2014.10.023.

Nepal, G.O. (2015), Post Disaster Needs Assessment.

Newmark, N. (1965), "Effects of earthquakes on dams and embankments", *Geotechnique*, 1965;15(2):139-160. https://doi.org/10.1680/geot.1965.15.2.139

Ö zmen, (2019), Modelling the variability in seismically induced slope displacements due to ground motion selection.

Padgett, J.E. and DesRoches, R. (2008), "Methodology for the development of analytical fragility curves for retrofitted bridges", *Earthq. Eng. Struct. D.*, **37**(8), 1157-1174. https://doi.org/10.1002/eqe.801.

Park, N.S. and Cho, S.E. (2017), "Development of fragility curves for seismic stability evaluation of cut-slopes", *Korean Geotech. Soc.*, **33**, 29-41. https://doi.org/10.7843/kgs.2017.33.7.29.

Park, S., Kim, W., Lee, J. and Baek, Y. (2018), "Case study on slope stability changes caused by earthquakes—focusing on Gyeongju 5.8 ML EQ", *Sustainability*, **10**(10). https://doi.org/10.3390/su10103441.

Perez, F.G., Haydon, W.D. and Wiegers, M.O. (2012), California Geological Survey Zones of Required Investigation for Earthquake-Induced Landslides – Livermore Valley, California: Digital Mapping Techniques 10-workshop proceedings U.S. Geological Survey Open-File Report 2012-1171.

PLAXIS-Manual (2022), PLAXIS 2D tutorial manual connect edition V22.

Raghunandan, M. and Liel, A.B. (2013), "Effect of ground motion duration on earthquake-induced structural collapse", *Struct. Saf.*, **41**, 119-133. https://doi.org/10.1016/j.strusafe.2012.12.002.

Rathje, E.M. and Antonakos, G. (2011), "A unified model for predicting earthquake-induced sliding displacements of rigid and flexible slopes", *Eng. Geol.*, **122**(1-2), 51-60. https://doi.org/10.1016/j.enggeo.2010.12.004.

Rocscience (2022), Slide 2 version 9.024, (Ed., Toronto, C.), rocscience.

Saygili, G. and Rathje, E.M. (2008), "Empirical predictive models for earthquake-induced sliding displacements of slopes", *J. Geotech. Geoenviron. Eng. ASCE*, **134**(6), 790-803. https://doi.org/10.1061/(ASCE)1090-0241(2008)134:6(79.

Saygili, G. and Rathje, E.M. (2009), "Probabilistically based seismic landslide hazard maps: An application in Southern California", *Eng. Geol.*, **109**(3-4), 183-194. https://doi.org/10.1016/j.enggeo.2009.08.004

Schuster, R.L. and Highland, L.M. (2001), Socioeconomic and Environmental Impacts of Landslides in the Western Hemisphere.

Seo, H., Lee, Y.J., Park, D. and Kim, B. (2022), "Seismic fragility assessment for cantilever retaining walls with various backfill slopes in South Korea", *Soil Dyn. Earthq. Eng.*, 161. https://doi.org/10.1016/j.soildyn.2022.107443.

Shou, K.J. and Wang, C.F. (2003), "Analysis of the Chiufengershan landslide triggered by the 1999 Chi-Chi earthquake in Taiwan", *Eng. Geol.*, 68(3), 237-250. https://doi.org/10.1016/S0013-7952(02)00230-2

Sun, C.G., Cho, C.S., Son, M. and Shin, J.S. (2012), "Correlations between shear wave velocity and in-situ penetration test results for Korean soil deposits", *Pure Appl. Geophys.*, **170**(3), 271-281. https://doi.org/10.1007/s00024-012-0516-2.

Terzaghi, K. and Peck, R.B. and Mesri, G. (1967), Soil Mechanics in Engineering Practice.

Travasarou, T. and Bray, J.D. (2003), "Optimal ground motion intensity measures for assessment of seismic slope displacements", *Proceedings of the 2003 Pacific Conference on Earthquake Engineering*.

Tsompanakis, Y., Lagaros, N.D., Psarropoulos, P.N. and Georgopoulos, E.C. (2010), "Probabilistic seismic slope stability assessment of geostructures", *Struct. Infrastruct. Eng.*, **6**(1-2), 179-191. https://doi.org/10.1080/15732470802664001.

Varnier, J.B. and Hatami, K. (2011), "Seismic Response of Reinforced Soil Retaining Walls: Is PGA-Based Design Adequate?", https://doi.org/10.1061/41183(418)28.

Wang, F., Fan, X., Yunus, A.P., Siva Subramanian, S., Alonso-Rodriguez, A., Dai, L., Xu, Q. and Huang, R. (2019), "Coseismic landslides triggered by the 2018 Hokkaido, Japan (Mw 6.6), earthquake: spatial distribution, controlling factors, and possible failure mechanism", *Landslides*, **16**(8), 1551-1566. https://doi.org/10.1007/s10346-019-01187-7.

Wei, M., Fang, S. J., Chen, S., Lin, R.Y., Huang, Y. and Yang, L. (2022), "Resilience assessment of road networks in the extremely severe disaster areas of the Wenchuan earthquake", *Front. Earth Sci*., **10**. https://doi.org/10.3389/feart.2022.834302.

Wen, Y.K., Ellingwood, B.R. and Bracci, J.M. (2004), Vulnerability function framework for consequence-based engineering.

Wu, X.Z. (2014), "Development of fragility functions for slope instability analysis", *Landslides*, **12**(1), 165-175. https://doi.org/10.1007/s10346-014-0536-3.

Zamiran, S. and Osouli, A. (2018), "Seismic motion response and fragility analyses of cantilever retaining walls with cohesive backfill", *Soils Found.*, **58**(2), 412-426. https://doi.org/10.1016/j.sandf.2018.02.010

Zhang, H.Y., Zhang, L.J., Wang, H.J. and Guan, C.N. (2018), "Influences of the duration and frequency content of ground motions on the seismic performance of high-rise intake towers", *Eng. Fail. Anal*., **91**, 481-495. https://doi.org/10.1016/j.engfailanal.2018.04.039

Zhang, Y., Chen, G., Wu, J., Zheng, L. and Zhuang, X. (2012), "Numerical simulation of seismic slope stability analysis based on tension-shear failure mechanism", *Geotech. Eng*., **43**(2).

Zhang, Y., Fan, J. and Fan, W. (2016), "Seismic fragility analysis of concrete bridge piers reinforced by steel fibers", *Adv. Struct. Eng*., **19**(5), 837-848. https://doi.org/10.1177/1369433216630440.

IC

Appendix A

Fig. A1 shows the D_{max} versus PGA for the V_S of 300 m/s. Figs. A2 and A3 present the D_{max} against I_A for the V_S of 150 m/s and 300 m/s, respectively.

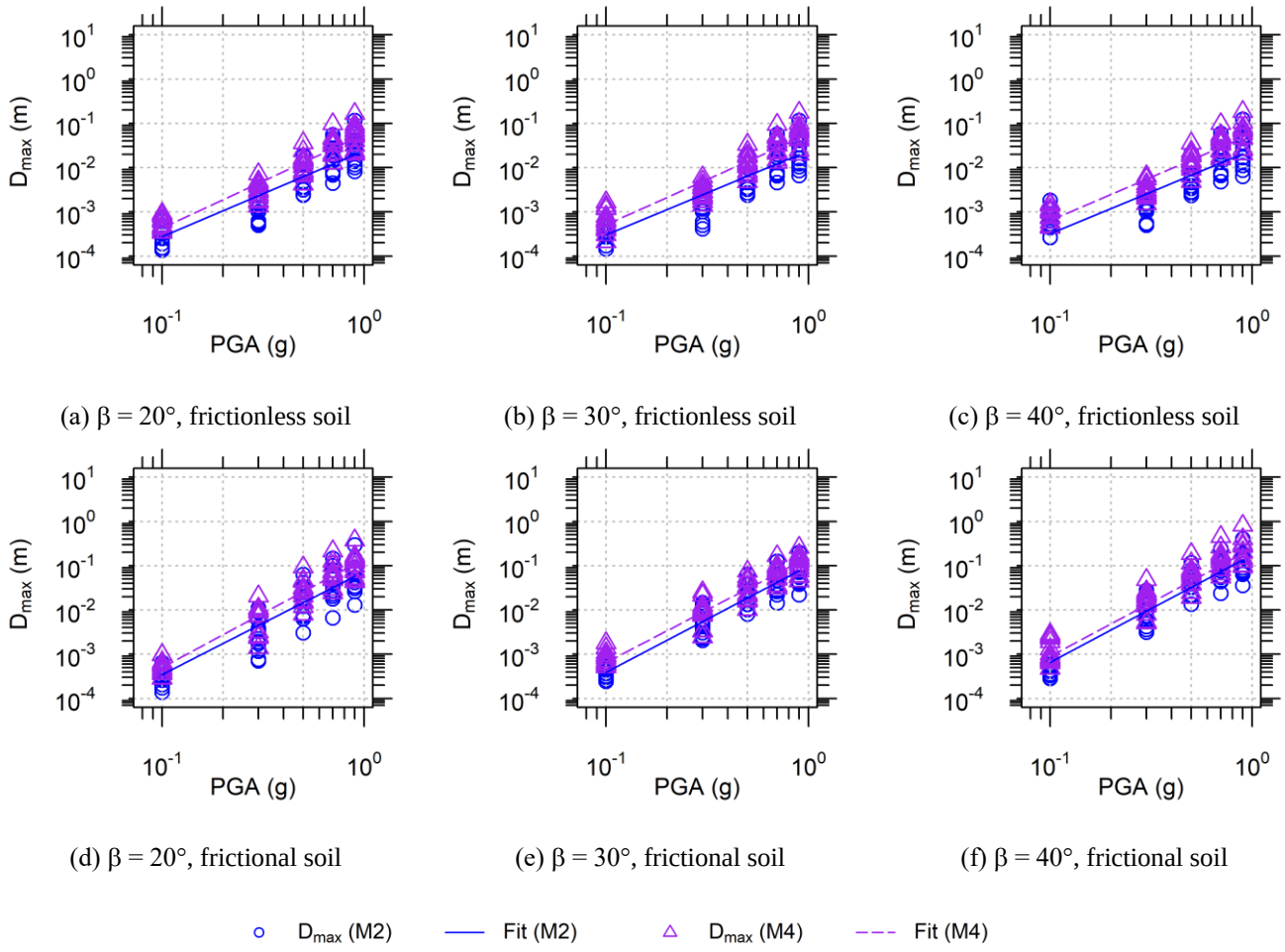

(a) β = 20°, frictionless soil (b) β = 30°, frictionless soil (c) β = 40°, frictionless soil

(d) β = 20°, frictional soil (e) β = 30°, frictional soil (f) β = 40°, frictional soil

Fig. A1 Maximum permanent slope displacement (D_{max}) against PGA for the four types of input ground and two types of soil with V_S of 300 m/s

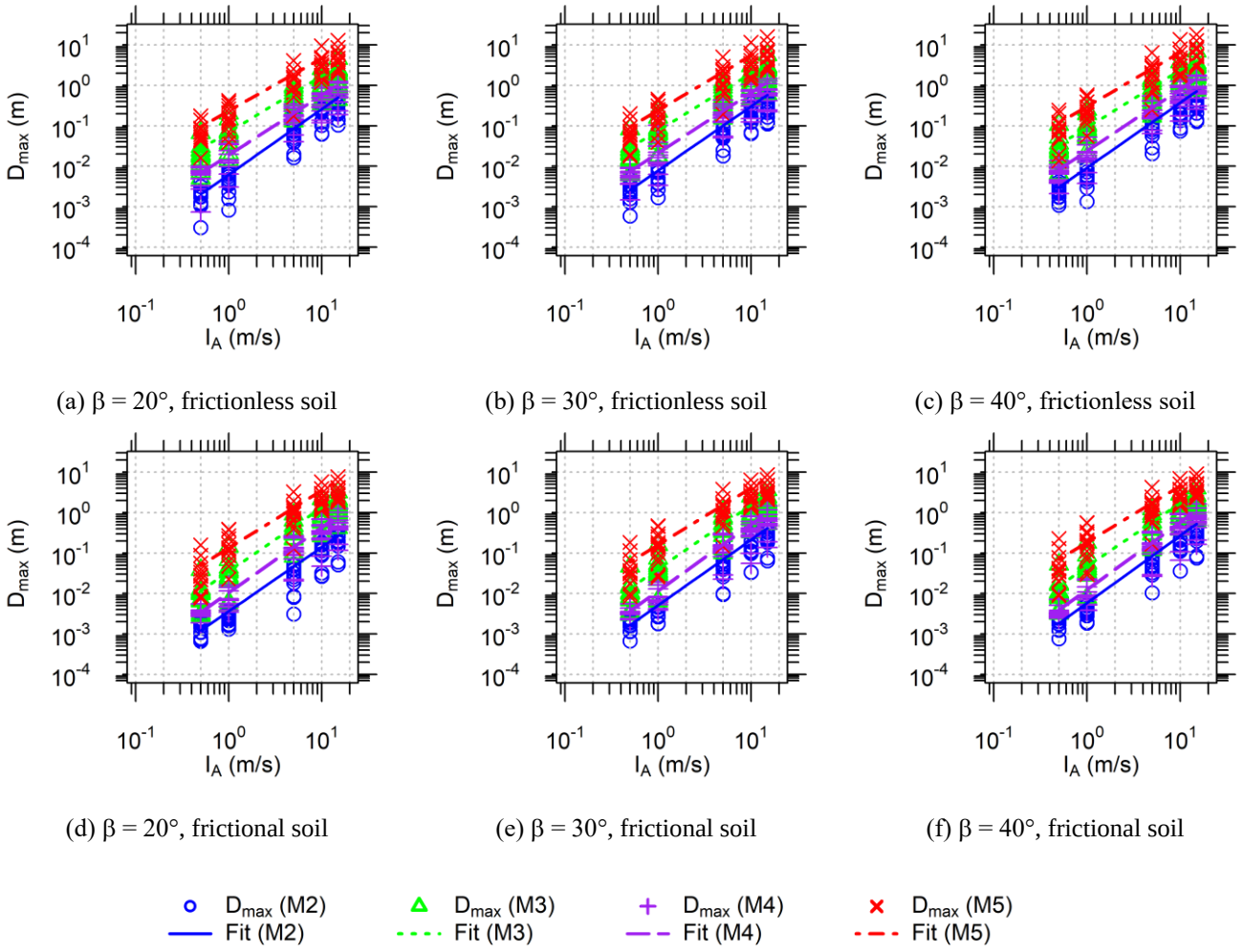

(a) β = 20°, frictionless soil (b) β = 30°, frictionless soil (c) β = 40°, frictionless soil

(d) β = 20°, frictional soil (e) β = 30°, frictional soil (f) β = 40°, frictional soil

Fig. A2 D_{max} against I_A for the four types of input motions and two type of soil with V_S = 150 m/s

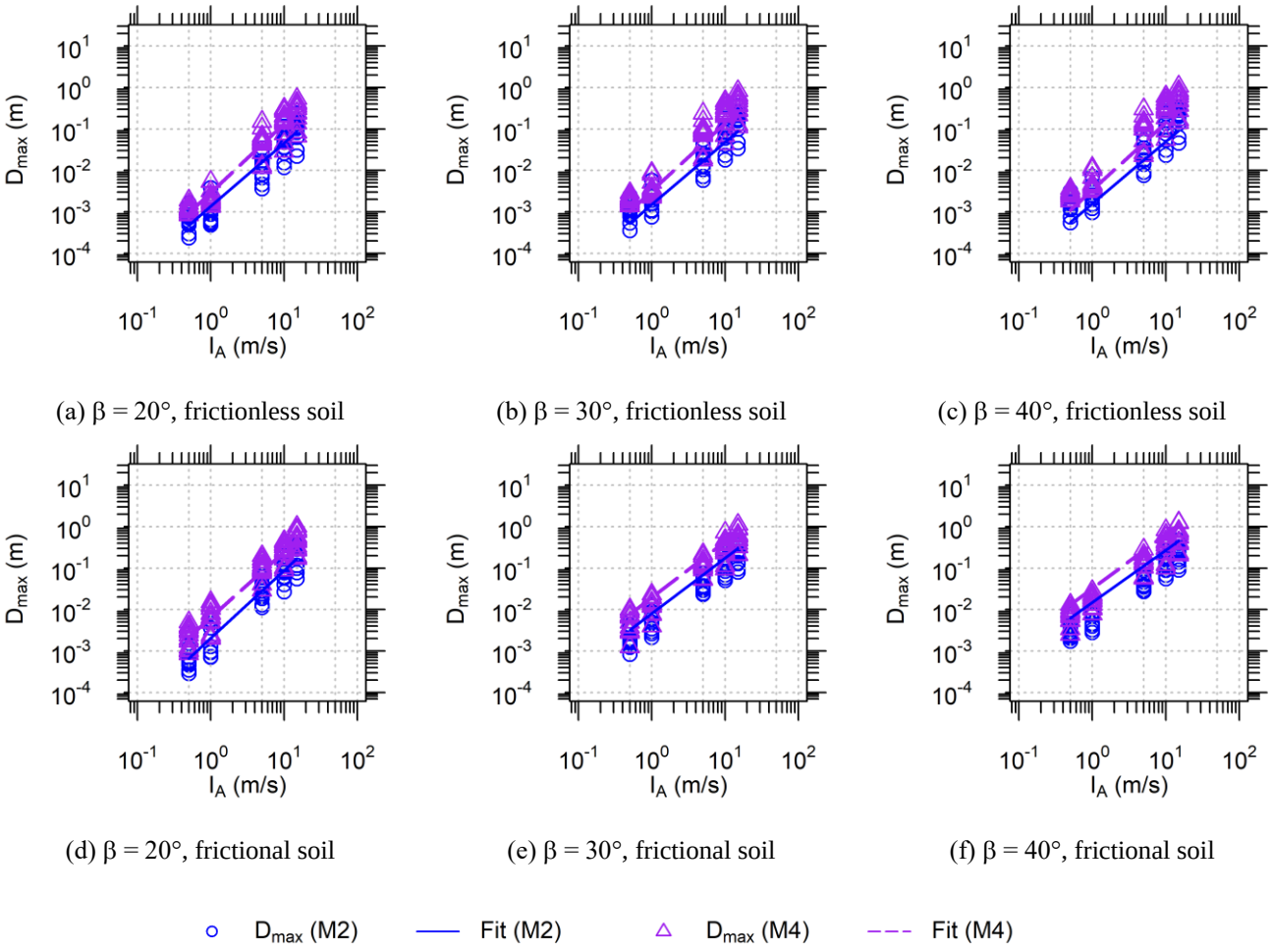

(a) β = 20°, frictionless soil (b) β = 30°, frictionless soil (c) β = 40°, frictionless soil

(d) β = 20°, frictional soil (e) β = 30°, frictional soil (f) β = 40°, frictional soil

Fig. A3 D_{max} against I_A for the two types of input motions and two type of soil with V_S = 300 m/s

Appendix B

Figs. B1 and B2 show fragility curves with respect to PGA at slope angles of 20°, and 40° subjected to all types of ground motions for soft frictionless and loose frictional soils. Fig. B3 displays the effect of slope angle on the fragility curves with respect to PGA subjected all types of ground motions for frictionless soil slopes. Fig. B4 presents the effect of ground motion type on the fragility curve with respect to PGA across three slope angles for frictional soil slopes.

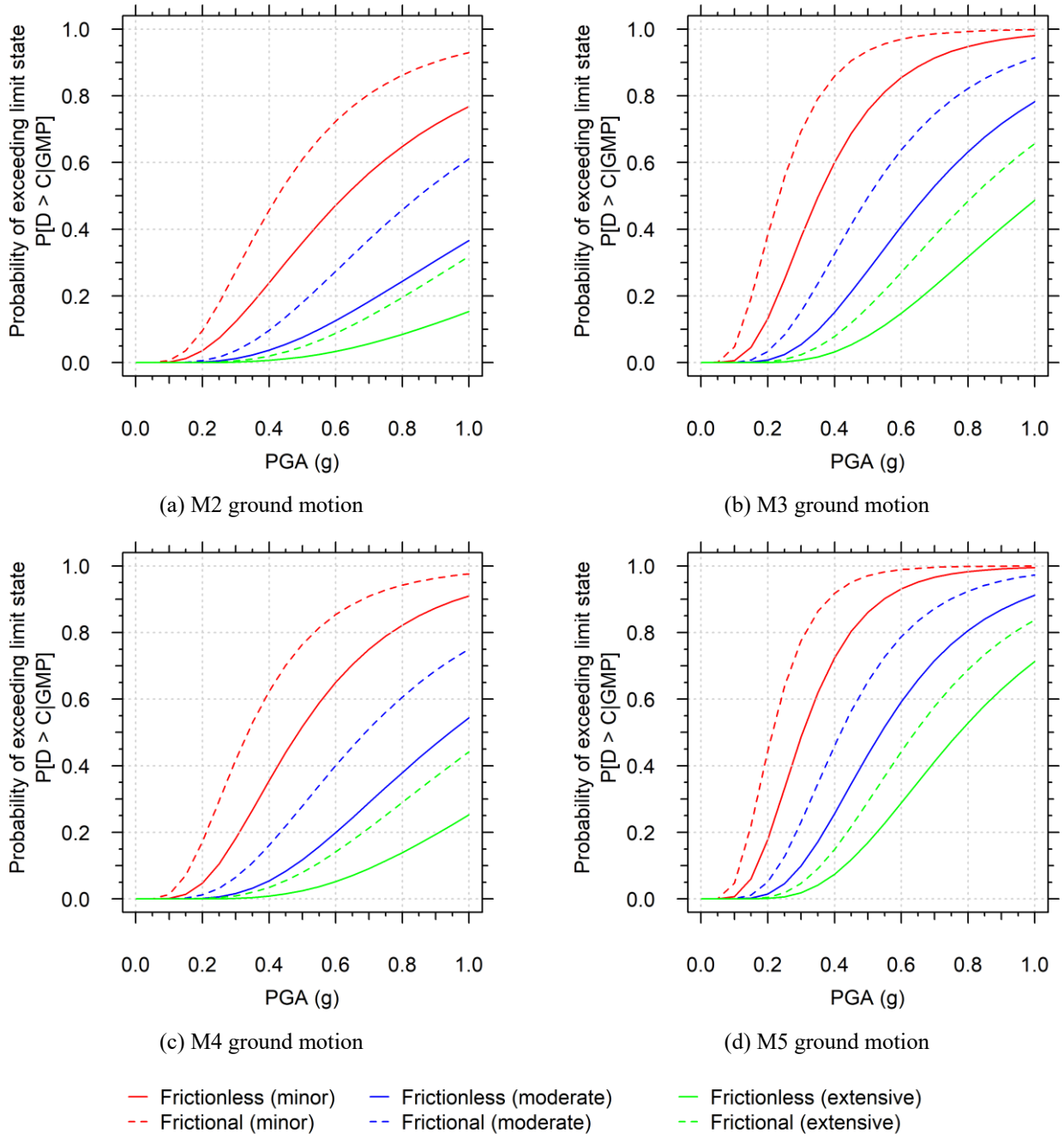

(a) M2 ground motion

(b) M3 ground motion

(c) M4 ground motion

(d) M5 ground motion

Fig. B1 Seismic fragility curves with respect to PGA for the frictional and frictionless soil slopes with β of 20° and V_S of 150 m/s subjected to the four types of ground motions

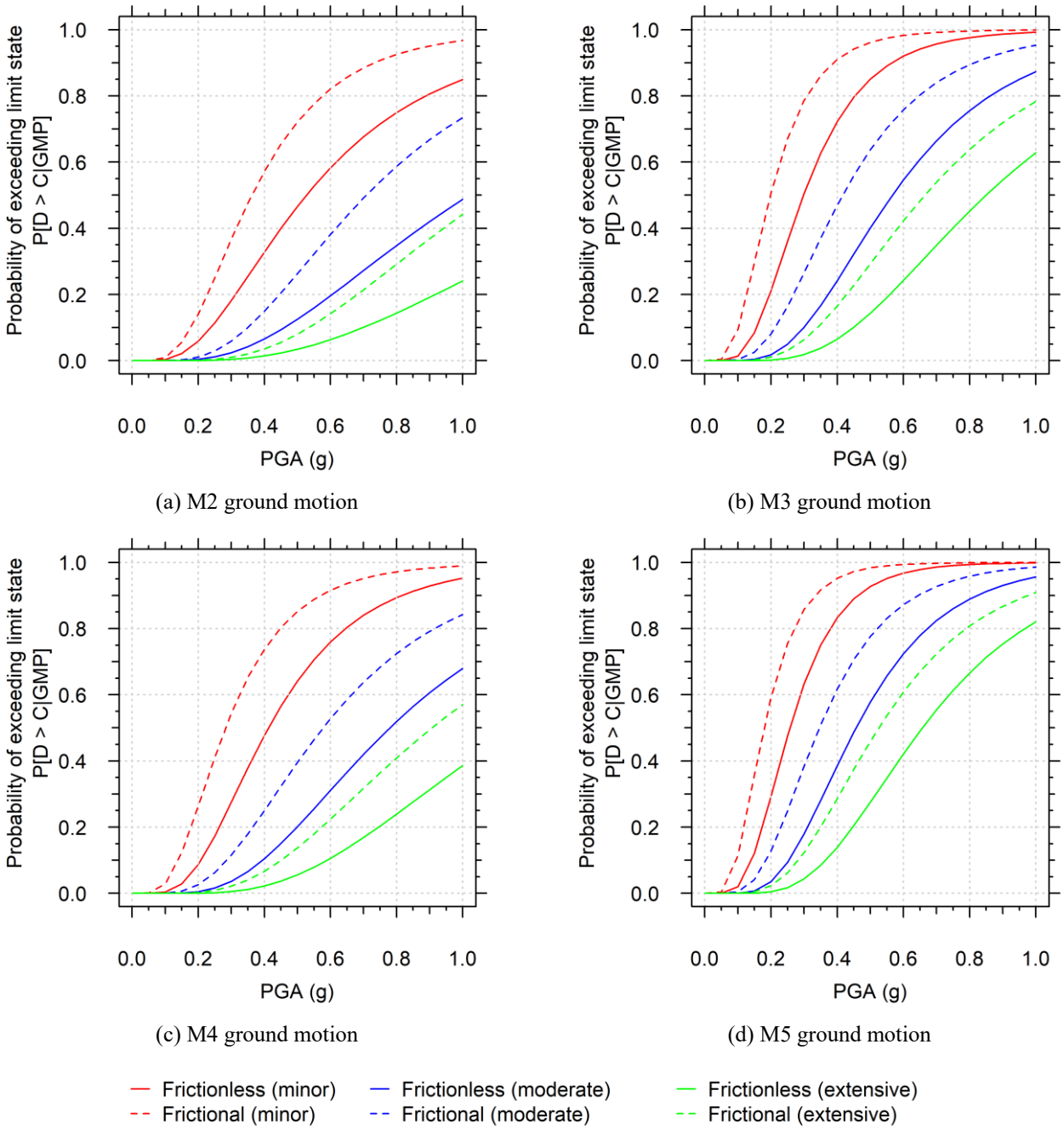

(a) M2 ground motion

(b) M3 ground motion

(c) M4 ground motion

(d) M5 ground motion

Fig. B2 Seismic fragility curves with respect to PGA for the frictional and frictionless soil slopes with β of 40° and V_S of 150 m/s subjected to the four types of ground motions

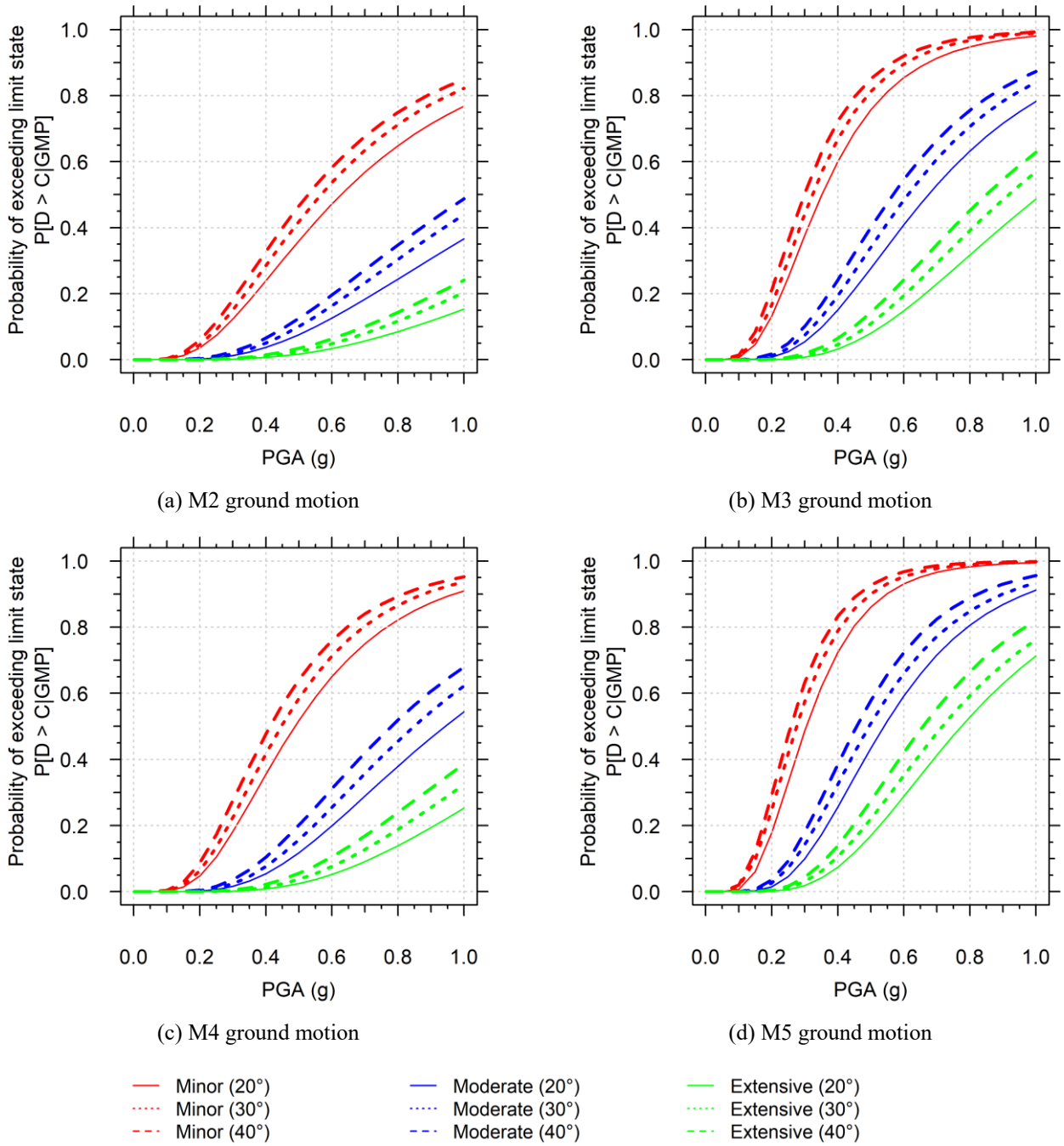

(a) M2 ground motion

(b) M3 ground motion

(c) M4 ground motion

(d) M5 ground motion

Fig. B3 Seismic fragility curves with respect to PGA for frictionless soil slopes with three β (= 20º, 30º, and 40º) and V_S of 150 m/s subjected to four types of ground motions

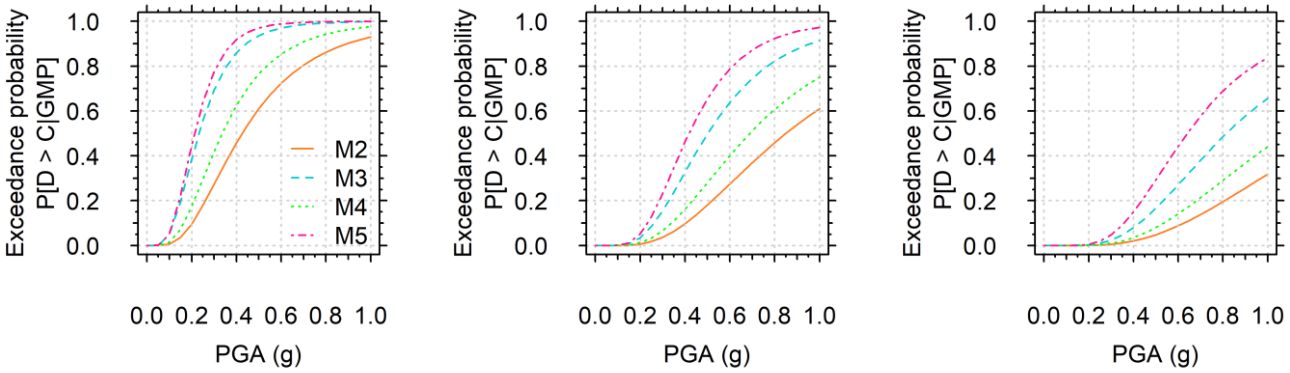

(a) Minor, β = 20° (b) Moderate, β = 20° (c) Extensive, β = 20°

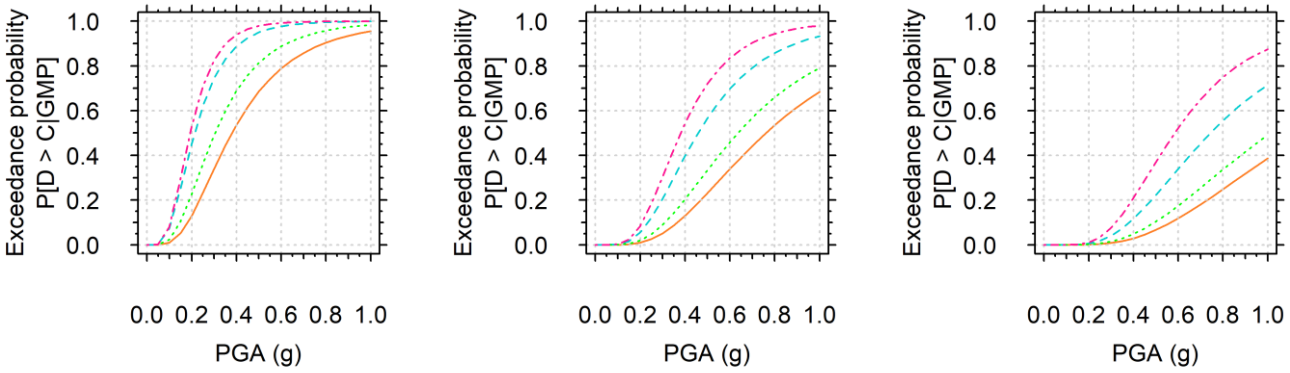

(d) Minor, β = 30° (e) Moderate, β = 30° (f) Extensive, β = 30°

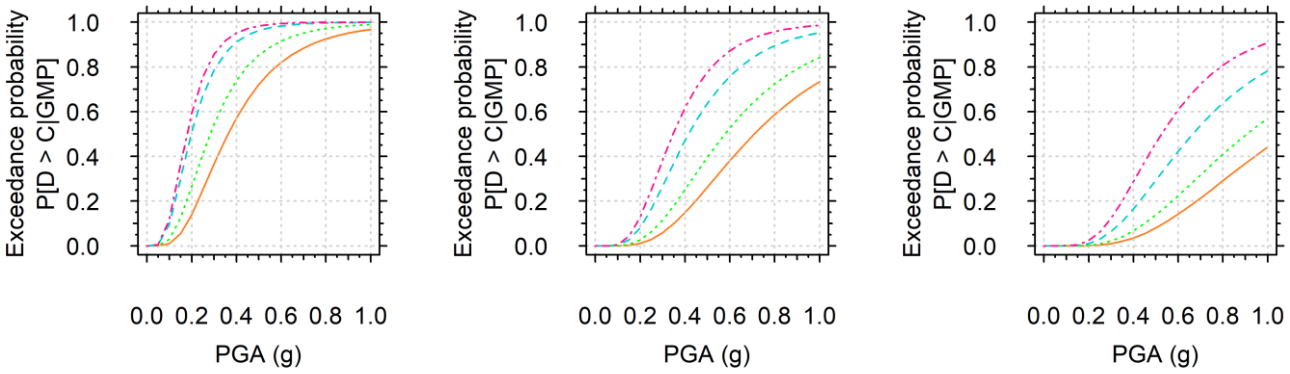

(g) Minor, β = 40° (h) Moderate, β = 40° (i) Extensive, β = 40°

Fig. B4 Seismic fragility curves with respect to PGA for the frictional soil slopes with V_S of 150 m/s subjected to four types of ground motions (M2, M3, M4, and M5) and for the limit states of minor (left column), moderate (center column), and extensive (right column) for β of 20° (a), (b), and (c); 30° (d), (e), and (f); and 40° (g), (h), and (i)

Appendix C

Figs. C1 through C3 present the fragility curves with respect to I_A at slope angles of 20°, 30°, and 40° subjected to all types of ground motions for soft frictionless and loose frictional soils. Fig. C4 shows the fragility curves for stiff frictionless and dense frictional soils across the three slope angles subjected to two types of ground motion.

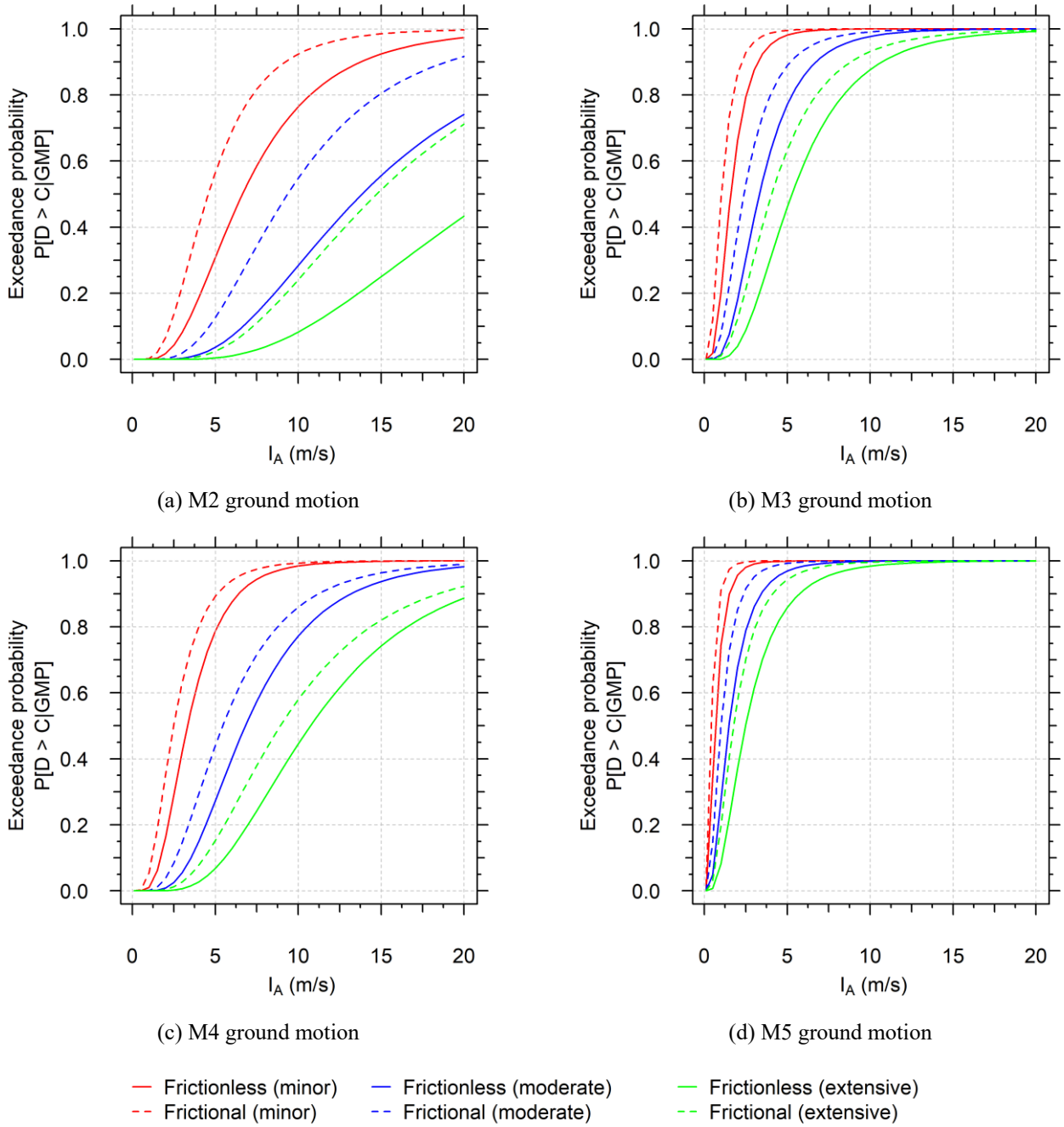

(a) M2 ground motion

(b) M3 ground motion

(c) M4 ground motion

(d) M5 ground motion

Fig. C1 Seismic fragility curves with respect to I_A for frictional and frictionless soil slopes with β of 20° and V_S of 150 m/s subjected to four types of ground motions

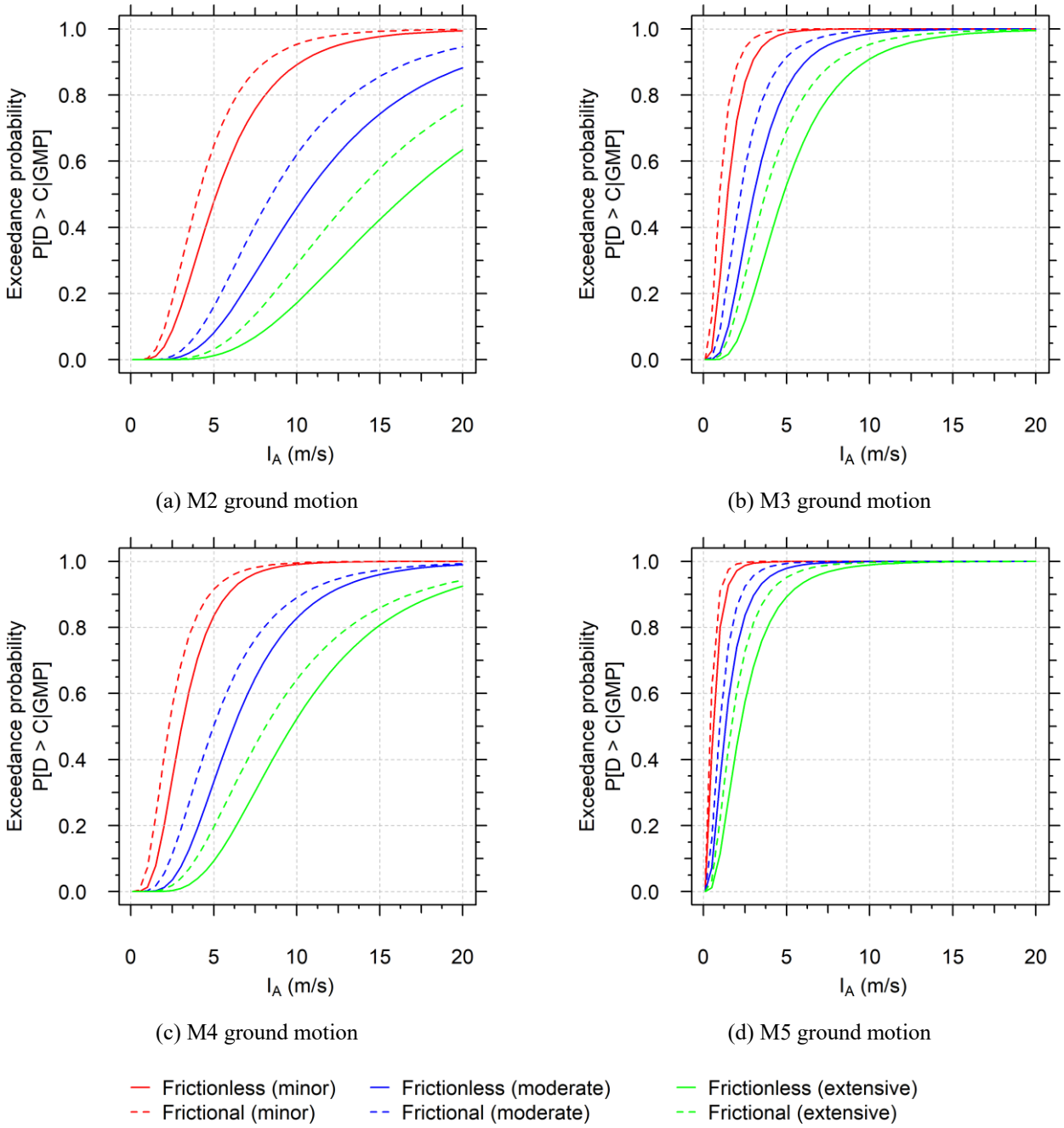

Fig. C2 Seismic fragility curves with respect to I_A for frictional and frictionless soil slopes with β of 30º and V_S of 150 m/s subjected to four types of ground motions

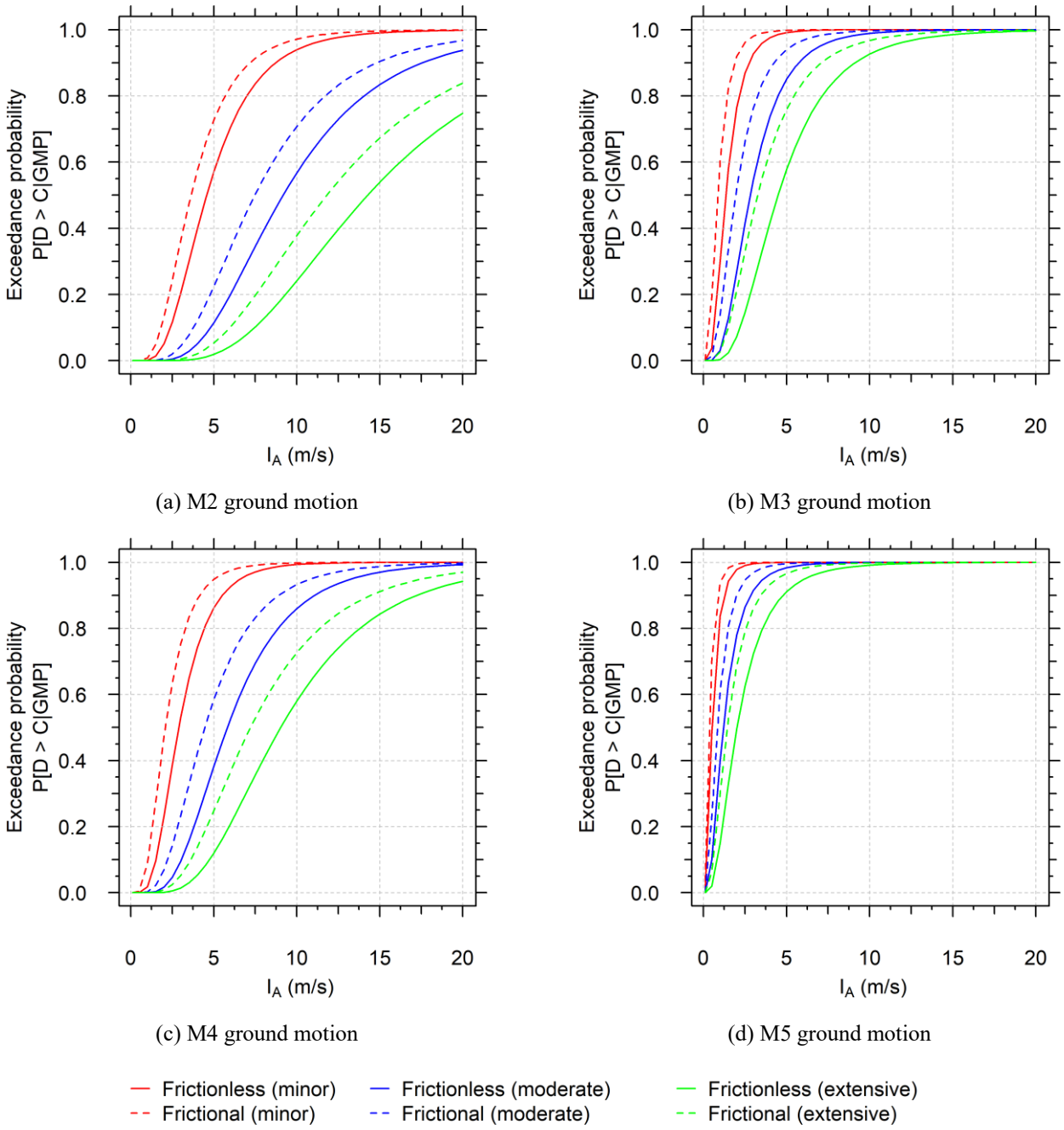

(a) M2 ground motion

(b) M3 ground motion

(c) M4 ground motion

(d) M5 ground motion

Fig. C3 Seismic fragility curves with respect to I_A for frictional and frictionless soil slopes with β of 40º and V_S of 150 m/s subjected to four types of ground motions

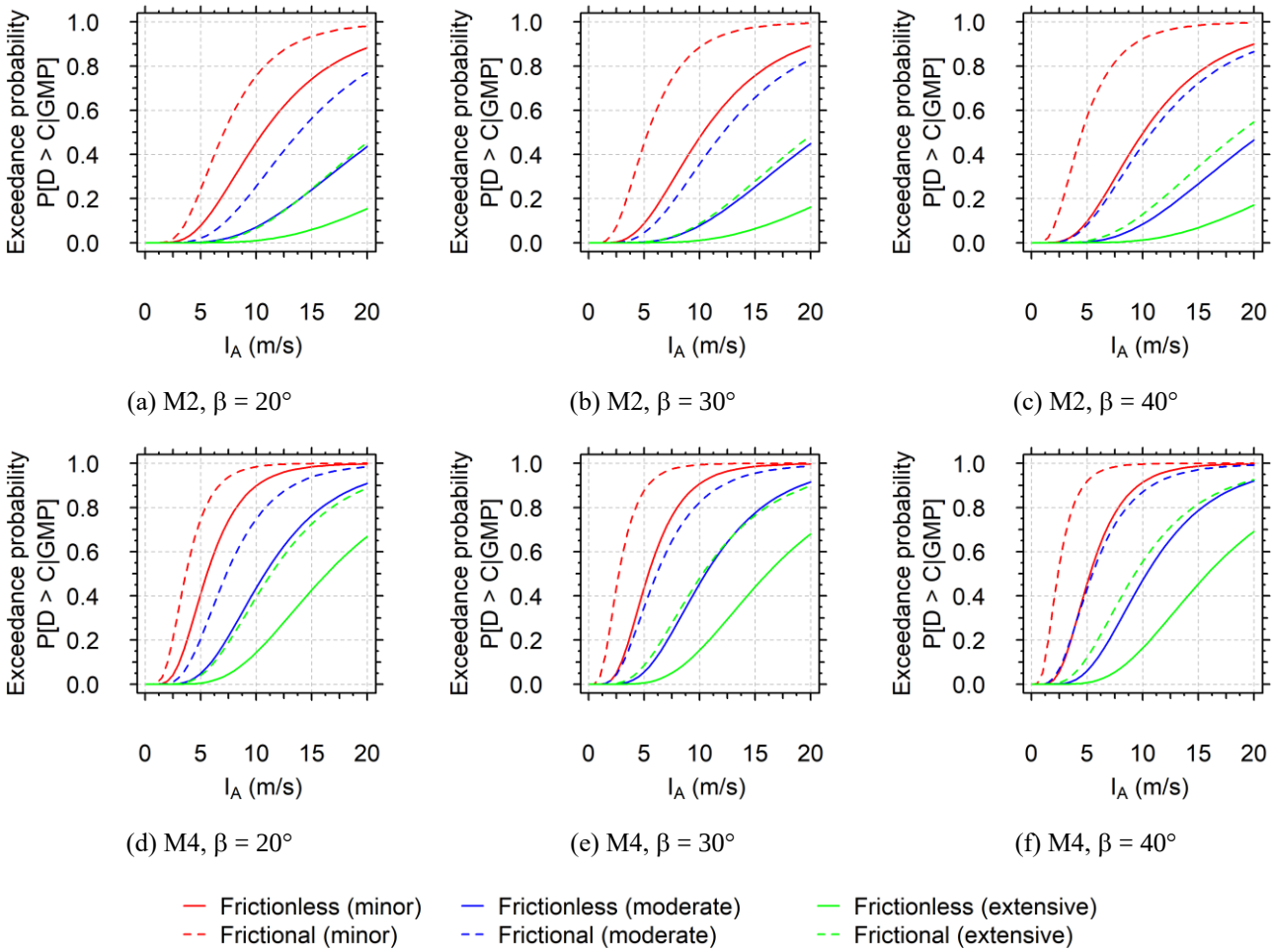

(a) M2, β = 20° (b) M2, β = 30° (c) M2, β = 40°

(d) M4, β = 20° (e) M4, β = 30° (f) M4, β = 40°

Fig. C4 Seismic fragility curves with respect to I_A for frictionless and frictional soil slopes with V_S of 300 m/s subjected to two types of ground motions

Appendix D

Figs. D1 and D2 present the fragility surfaces for the loose frictional and soft frictionless soil slopes with the slope angle of 30° and 40°, respectively, subjected to M2 ground motion type. Figs. D3 through D5 show the fragility surfaces for the loose frictional and soft frictionless soil slopes with the slope angle of 20°, 30°, and 40°, respectively, subjected to M3 ground motion type. Figs. D6 through D8 display the fragility surfaces for the loose frictional and soft frictionless soil slopes with the slope angle of 20°, 30°, and 40°, respectively, subjected to M4 ground motion type. Figs. D9 through D11 illustrate the fragility surfaces for the loose frictional and soft frictionless soil slopes with the slope angle of 20°, 30°, and 40°, respectively, subjected to M5 ground motion type.

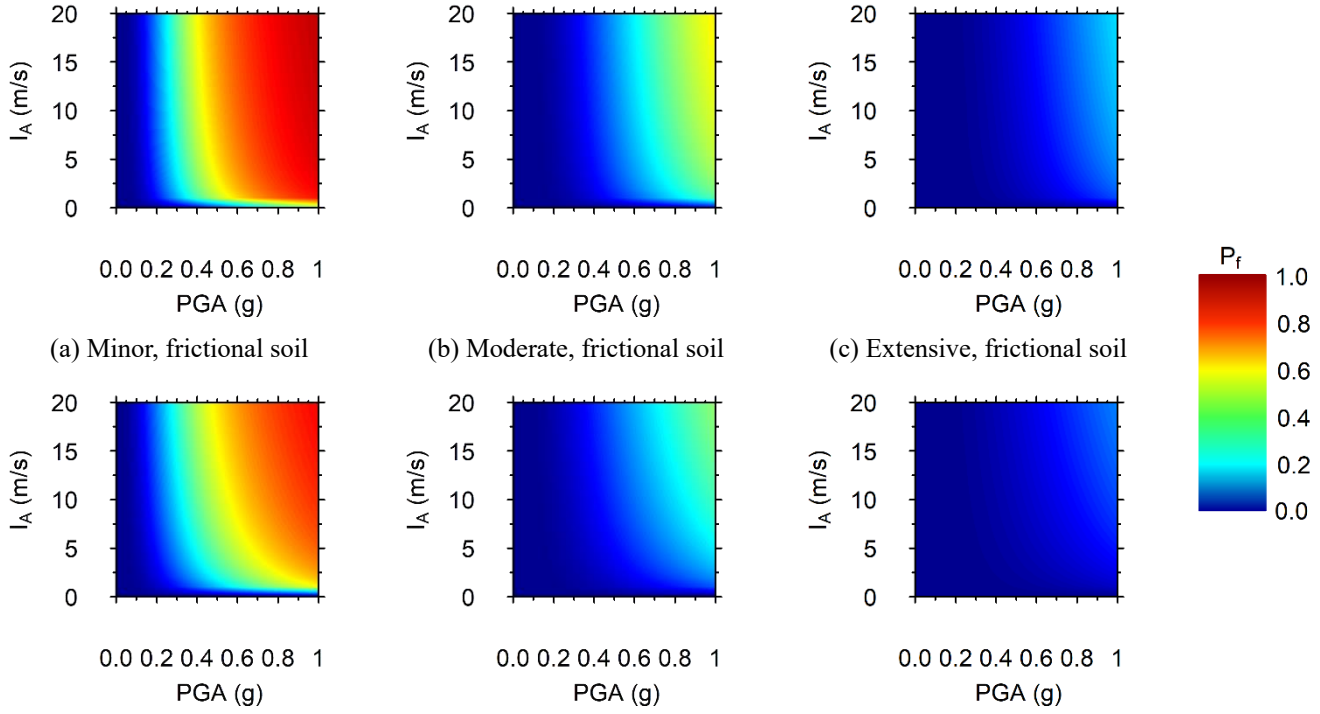

(a) Minor, frictional soil (b) Moderate, frictional soil (c) Extensive, frictional soil

(d) Minor, frictionless soil (e) Moderate, frictionless soil (f) Extensive, frictionless soil

Fig. D1 P_f for the two GMPs (PGA and I_A) for for the three limit states the frictional and the frictionless soil slopes with V_S = 150 m/s and β = 30º subjected to the M2 motion

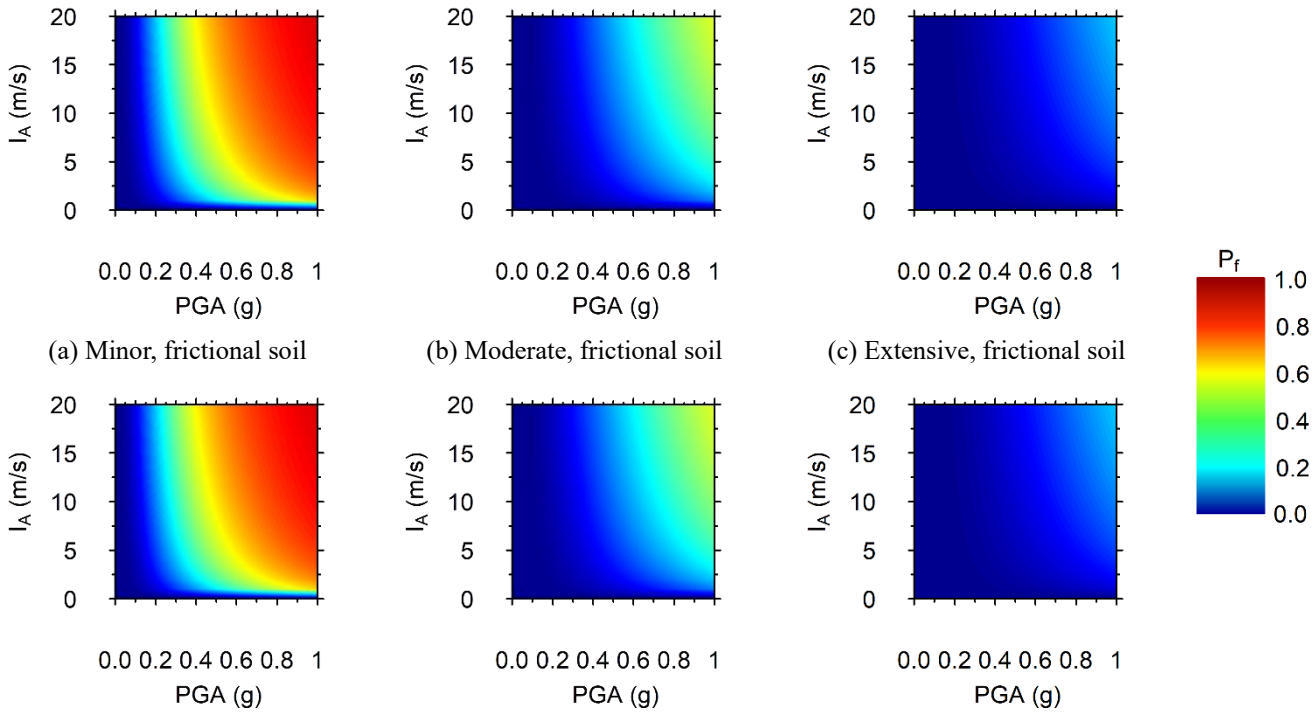

(a) Minor, frictional soil (b) Moderate, frictional soil (c) Extensive, frictional soil

(d) Minor, frictionless soil (e) Moderate, frictionless soil (f) Extensive, frictionless soil

Fig. D2 P_f for the two GMPs (PGA and I_A) for the three limit states the frictional and the frictionless soil slopes with V_S = 150 m/s and β = 40º subjected to the M2 motion

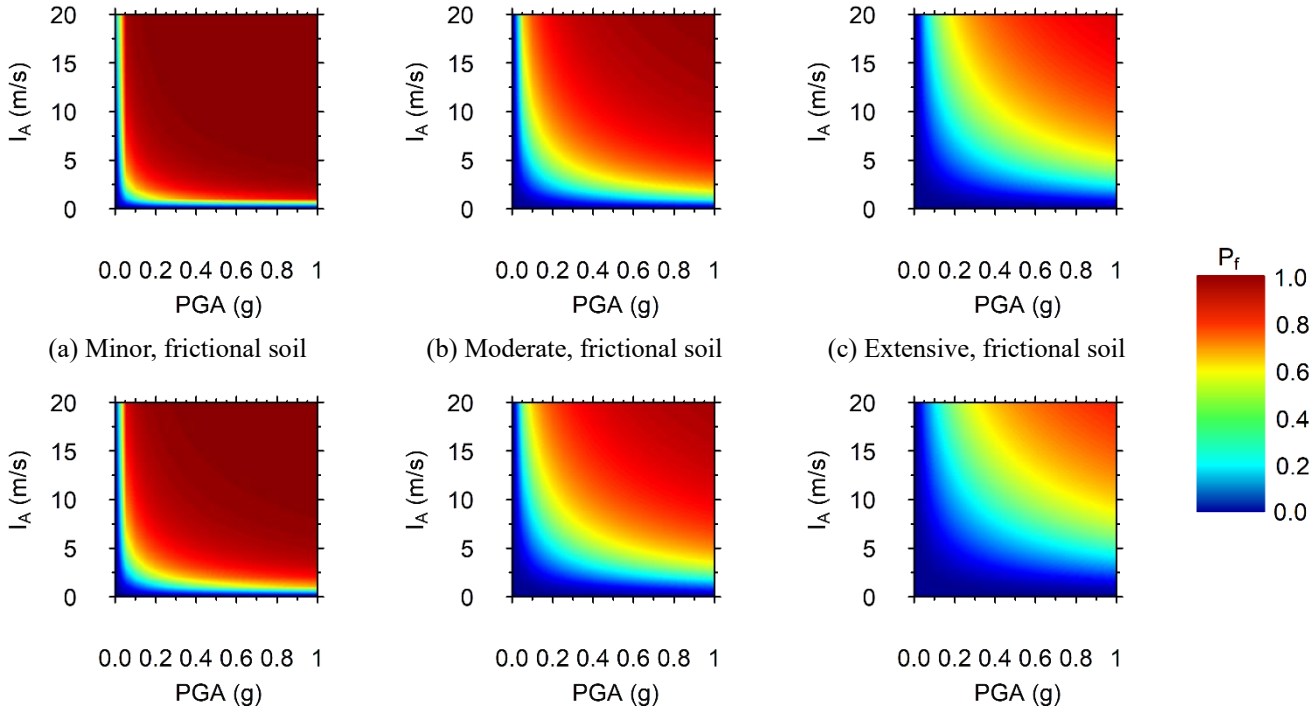

(a) Minor, frictional soil (b) Moderate, frictional soil (c) Extensive, frictional soil

(d) Minor, frictionless soil (e) Moderate, frictionless soil (f) Extensive, frictionless soil

Fig. D3 P_f for the two GMPs (PGA and I_A) for the three limit states the frictional and the frictionless soil slopes with V_S = 150 m/s and β = 20º subjected to the M3 motion

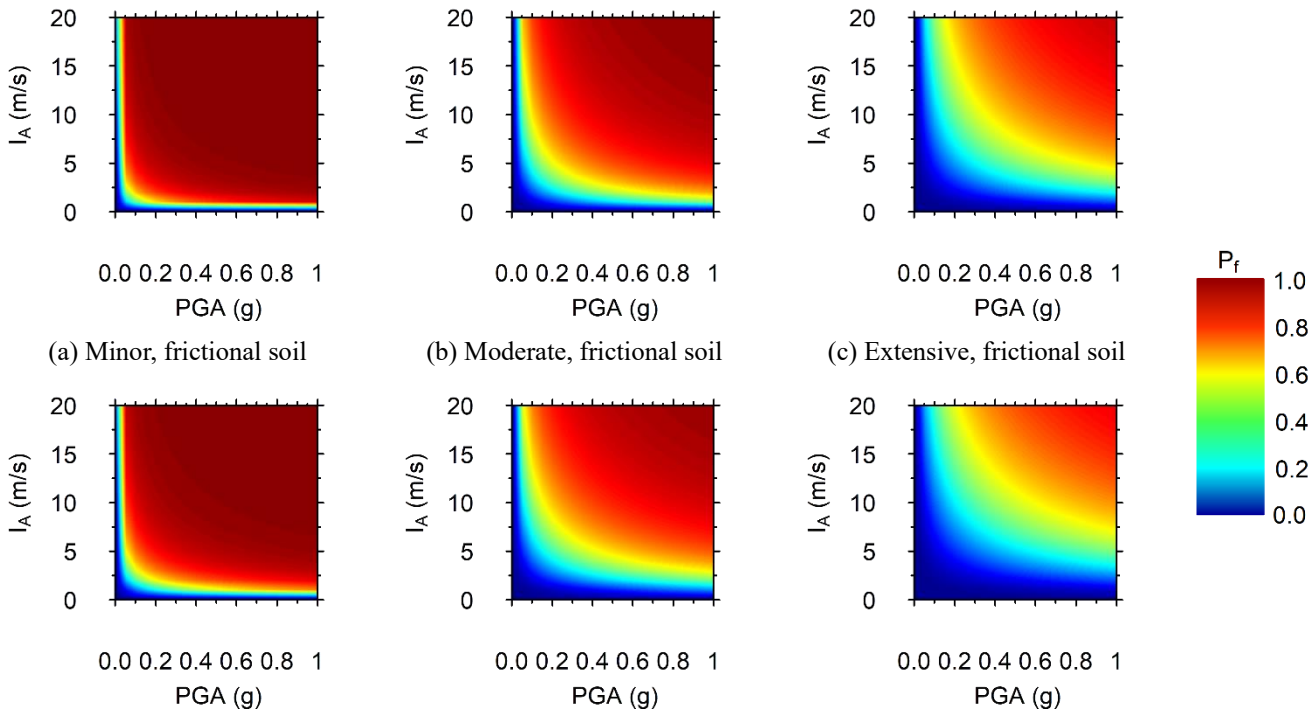

(a) Minor, frictional soil (b) Moderate, frictional soil (c) Extensive, frictional soil

(d) Minor, frictionless soil (e) Moderate, frictionless soil (f) Extensive, frictionless soil

Fig. D4 P_f for the two GMPs (PGA and I_A) for the three limit states the frictional and the frictionless soil slopes with V_S = 150 m/s and β = 30º subjected to the M3 motion

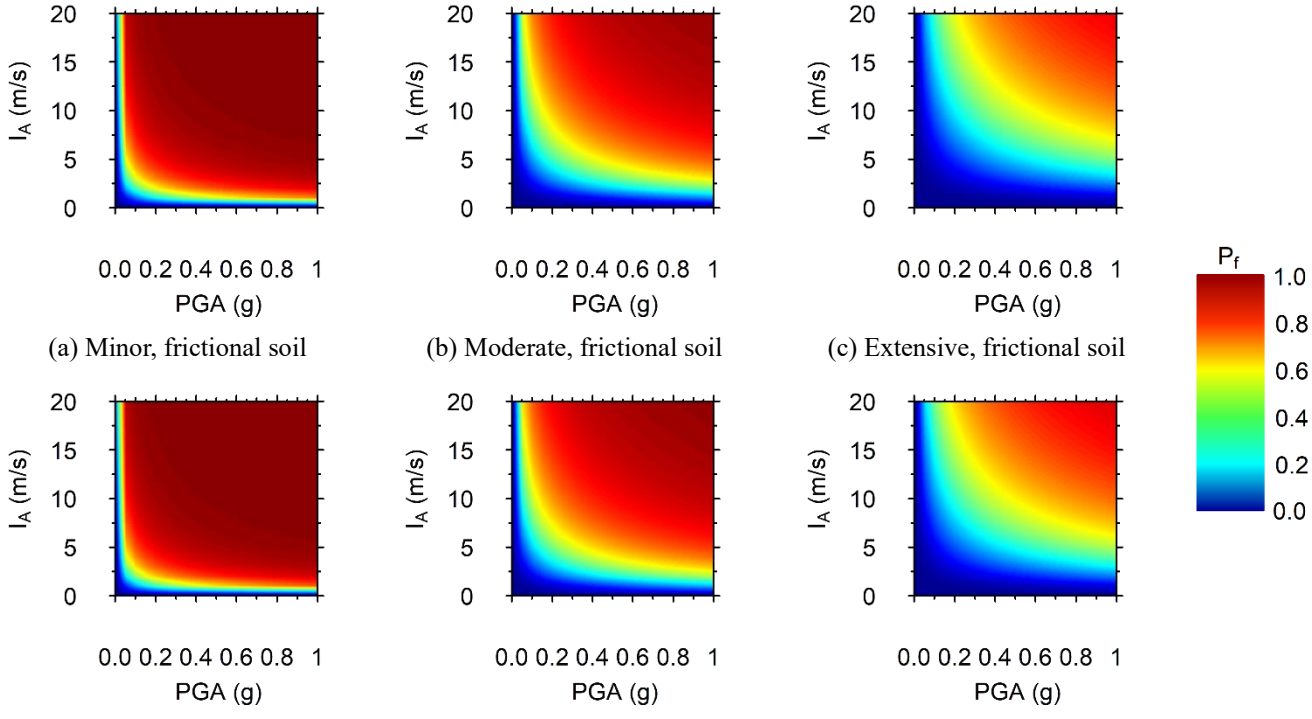

(a) Minor, frictional soil (b) Moderate, frictional soil (c) Extensive, frictional soil

(d) Minor, frictionless soil (e) Moderate, frictionless soil (f) Extensive, frictionless soil

Fig. D5 P_f for the two GMPs (PGA and I_A) for the three limit states the frictional and the frictionless soil slopes with V_S = 150 m/s and β = 40º subjected to the M3 motion

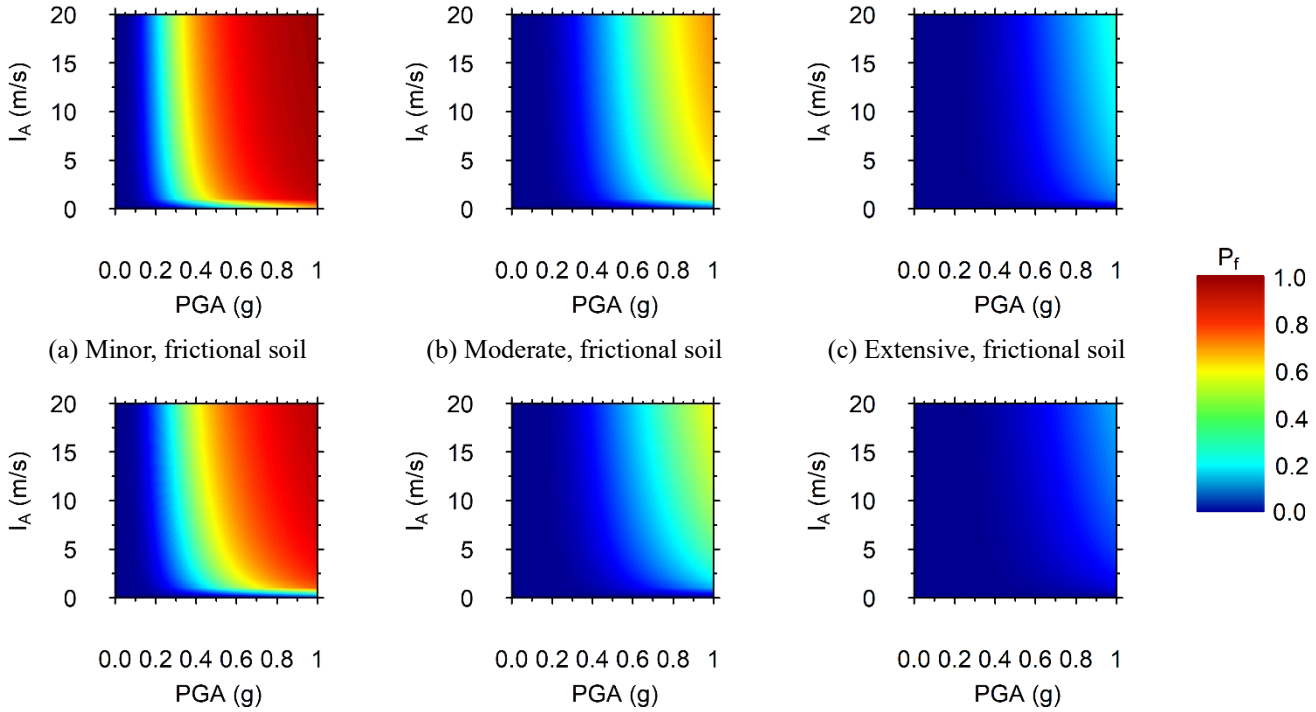

(a) Minor, frictional soil (b) Moderate, frictional soil (c) Extensive, frictional soil

(d) Minor, frictionless soil (e) Moderate, frictionless soil (f) Extensive, frictionless soil

Fig. D6 P_f for the two GMPs (PGA and I_A) for the three limit states the frictional and the frictionless soil slopes with V_S = 150 m/s and β = 20º subjected to the M4 motion

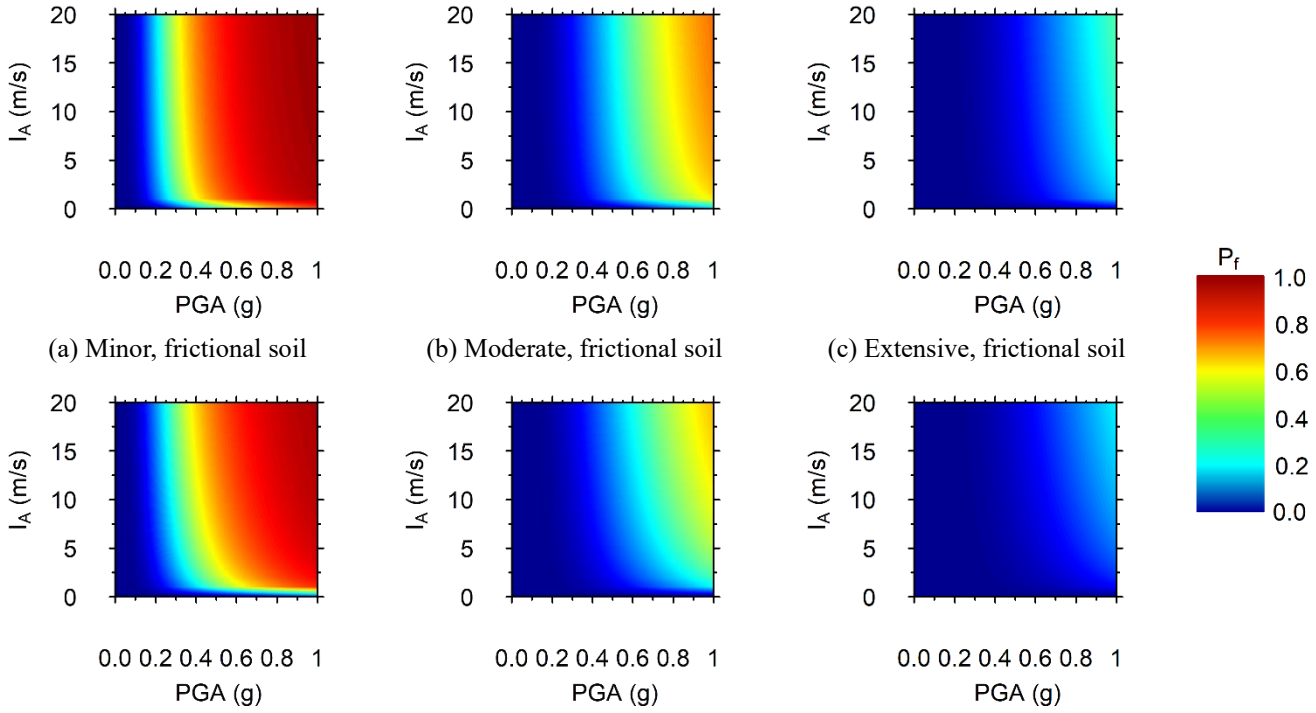

(a) Minor, frictional soil (b) Moderate, frictional soil (c) Extensive, frictional soil

(d) Minor, frictionless soil (e) Moderate, frictionless soil (f) Extensive, frictionless soil

Fig. D7 P_f for the two GMPs (PGA and I_A) for the three limit states the frictional and the frictionless soil slopes with V_S = 150 m/s and β= 30º subjected to the M4 motion.

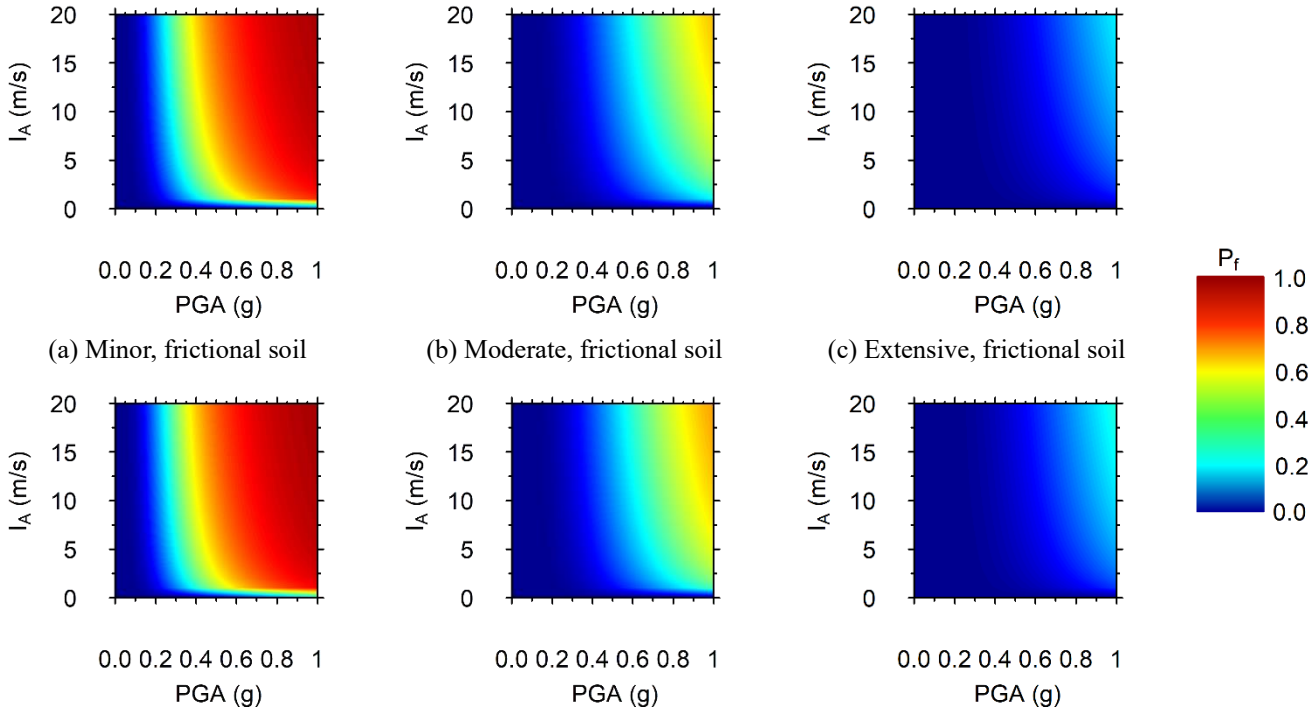

(a) Minor, frictional soil (b) Moderate, frictional soil (c) Extensive, frictional soil

(d) Minor, frictionless soil (e) Moderate, frictionless soil (f) Extensive, frictionless soil

Fig. D8 P_f for the two GMPs (PGA and I_A) for the three limit states the frictional and the frictionless soil slopes with V_S = 150 m/s and β = 40º subjected to the M4 motion

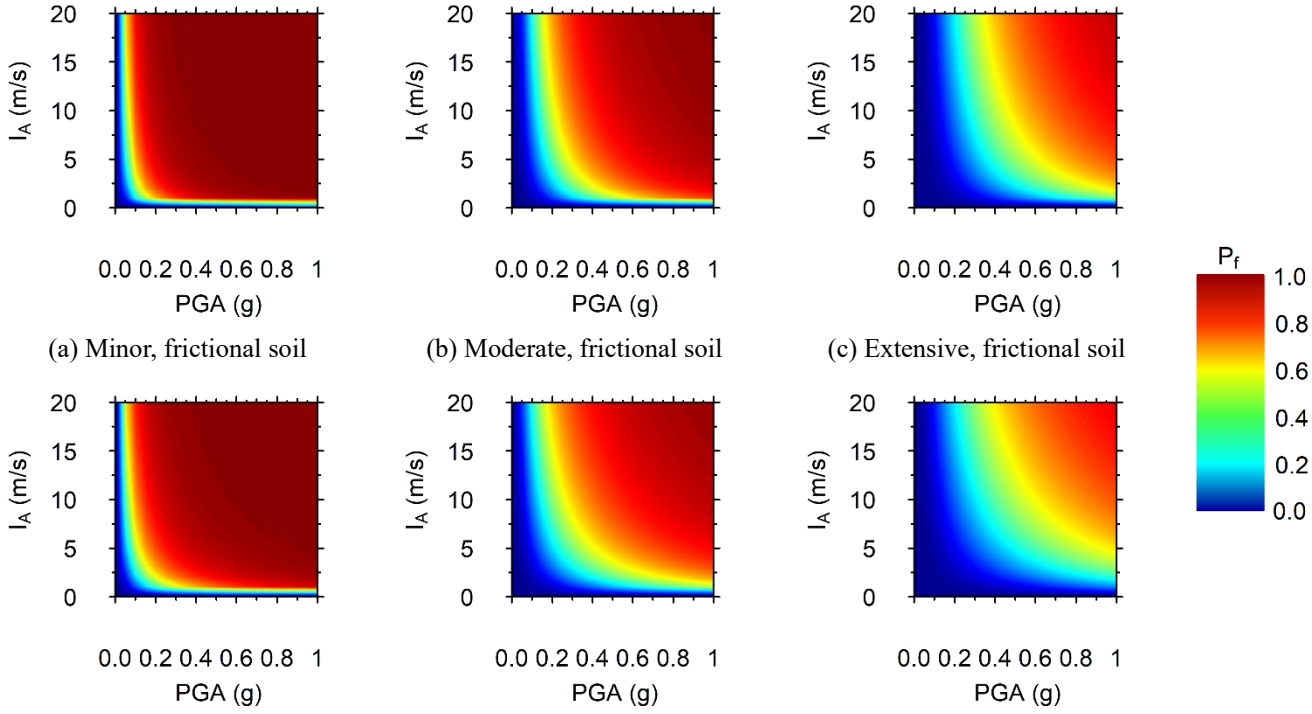

(a) Minor, frictional soil (b) Moderate, frictional soil (c) Extensive, frictional soil

(d) Minor, frictionless soil (e) Moderate, frictionless soil (f) Extensive, frictionless soil

Fig. D9 P_f for the two GMPs (PGA and I_A) for the three limit states the frictional and the frictionless soil slopes with V_S = 150 m/s and β = 20º subjected to the M5 motion.

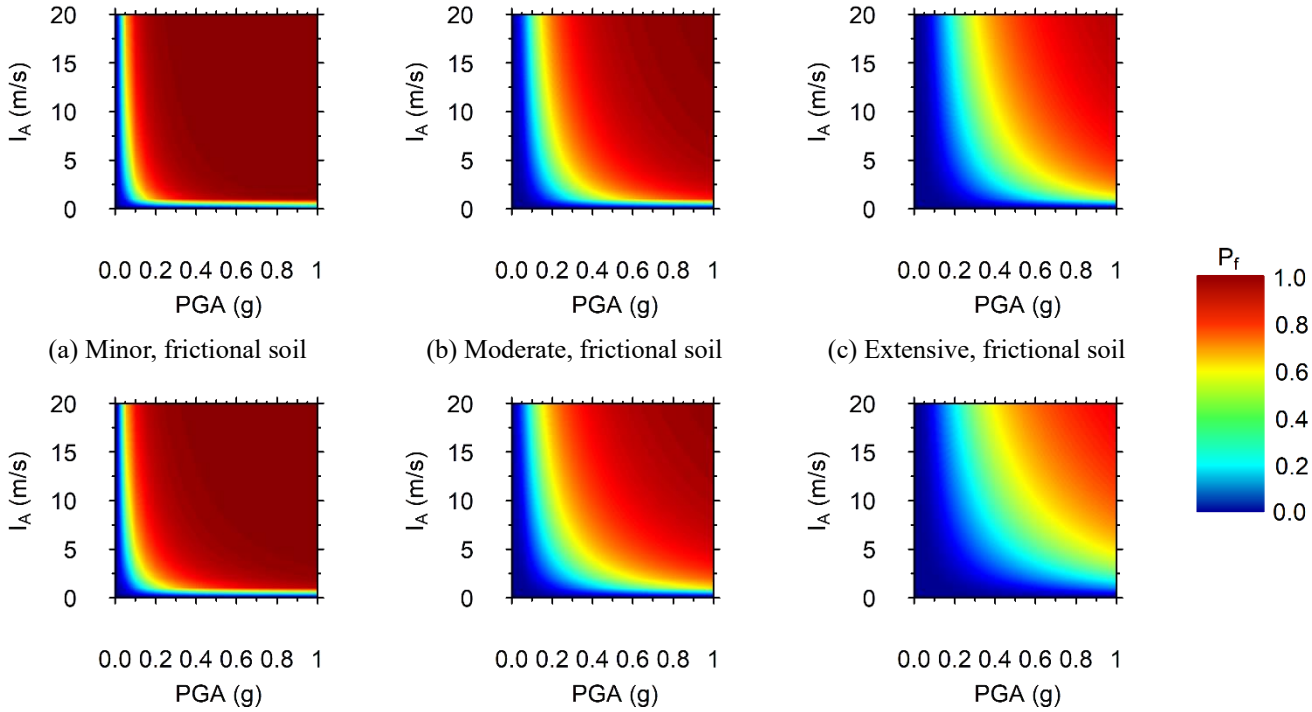

(a) Minor, frictional soil (b) Moderate, frictional soil (c) Extensive, frictional soil

(d) Minor, frictionless soil (e) Moderate, frictionless soil (f) Extensive, frictionless soil

Fig. D10 P_f for the two GMPs (PGA and I_A) for the three limit states the frictional and the frictionless soil slopes with V_S = 150 m/s and β = 30º subjected to the M5 motion.

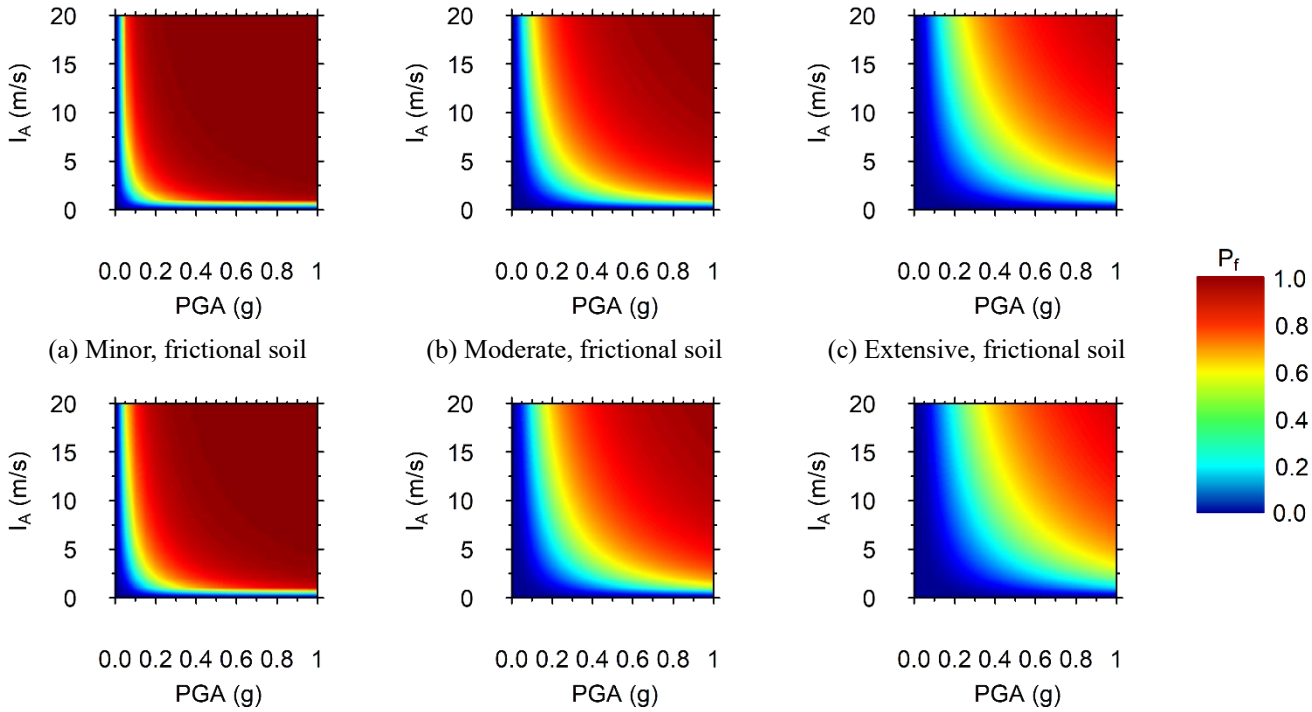

(a) Minor, frictional soil (b) Moderate, frictional soil (c) Extensive, frictional soil

(d) Minor, frictionless soil (e) Moderate, frictionless soil (f) Extensive, frictionless soil

Fig. D11 P_f for the two GMPs (PGA and I_A) for the three limit states the frictional and the frictionless soil slopes with V_S = 150 m/s and β = 40º subjected to the M5 motion.

Appendix E

Figs. E1 through E3 show the seismic fragility surfaces for the dense frictional and stiff frictionless soil slopes with the slope angle of 20°, 30°, and 40°, respectively, subjected to M2 ground motion type. Figs. E4 through E6 present the seismic fragility surfaces for the dense frictional and stiff frictionless soil slopes with the slope angle of 20°, 30°, and 40°, respectively, subjected to M4 ground motion type.

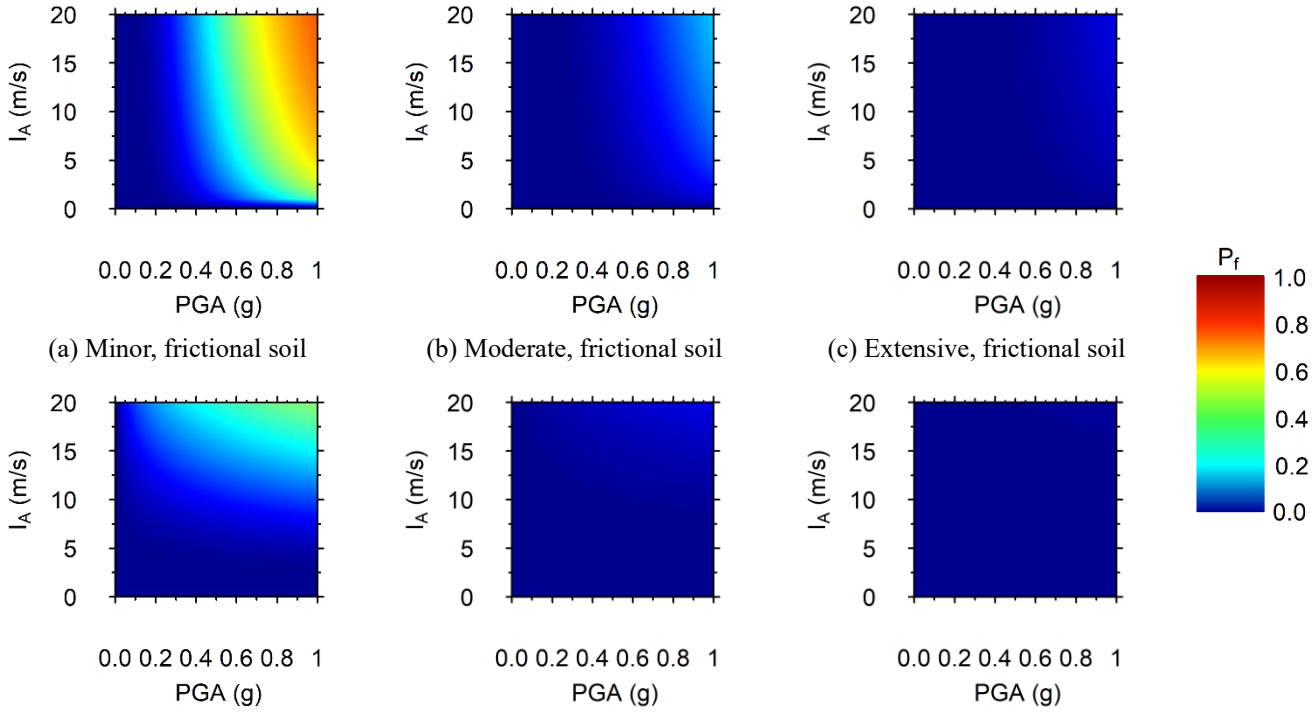

(a) Minor, frictional soil (b) Moderate, frictional soil (c) Extensive, frictional soil

(d) Minor, frictionless soil (e) Moderate, frictionless soil (f) Extensive, frictionless soil

Fig. E1 P_f for the two GMPs (PGA and I_A) for the three limit states the frictional and the frictionless soil slopes with V_S = 300 m/s and β = 20º subjected to the M2 motion.

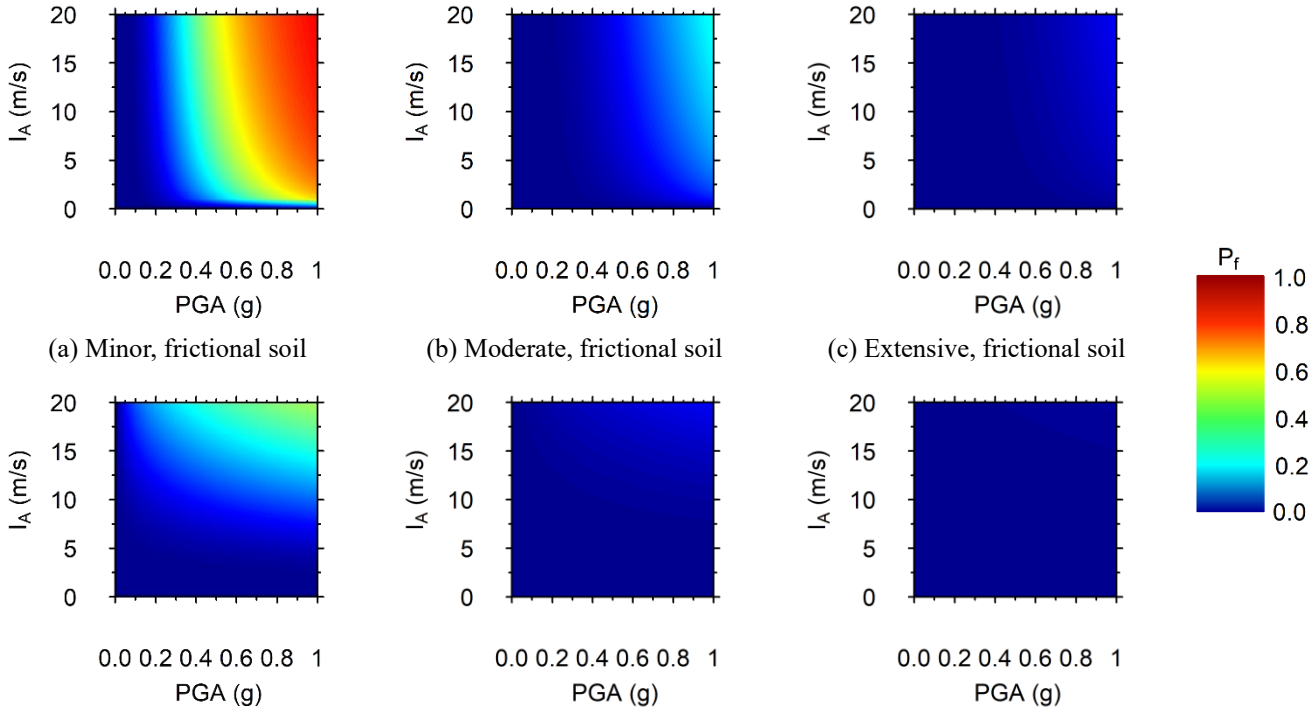

(a) Minor, frictional soil (b) Moderate, frictional soil (c) Extensive, frictional soil

(d) Minor, frictionless soil (e) Moderate, frictionless soil (f) Extensive, frictionless soil

Fig. E2 P_f for the two GMPs (PGA and I_A) for the three limit states the frictional and the frictionless soil slopes with V_S = 300 m/s and β = 300º subjected to the M2 motion.

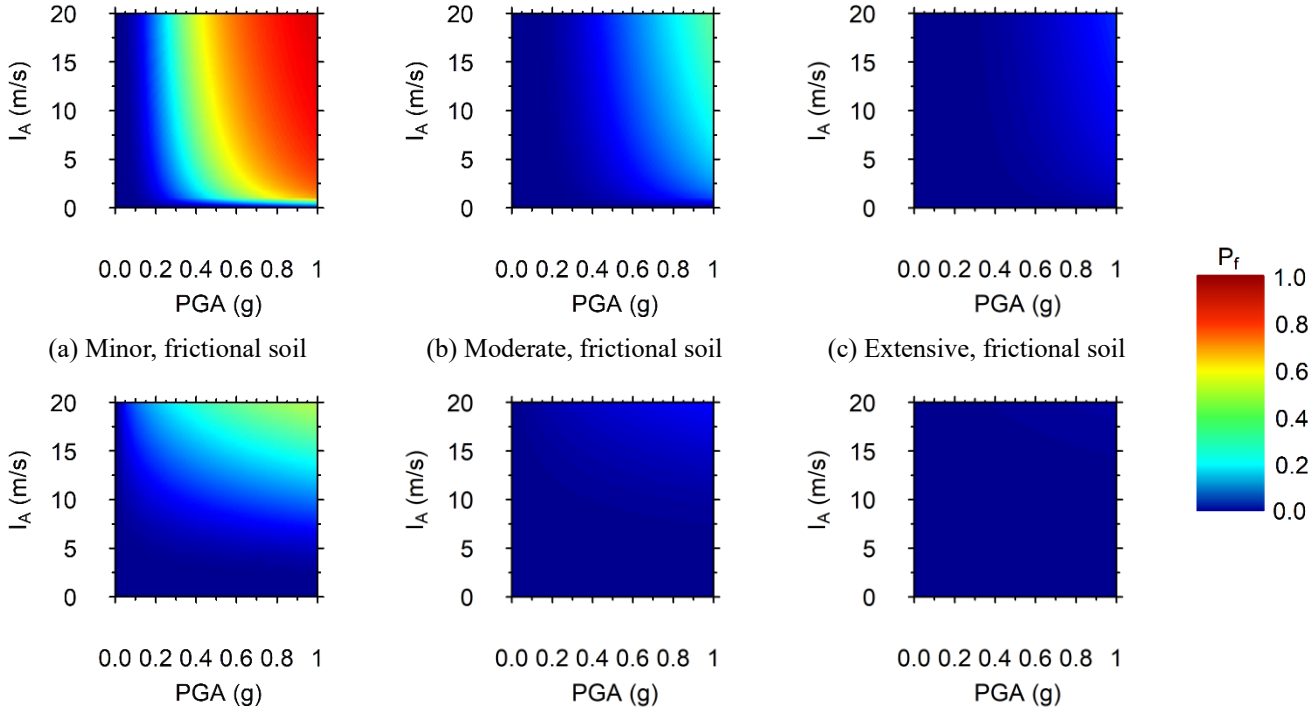

(a) Minor, frictional soil (b) Moderate, frictional soil (c) Extensive, frictional soil

(d) Minor, frictionless soil (e) Moderate, frictionless soil (f) Extensive, frictionless soil

Fig. E3 P_f for the two GMPs (PGA and I_A) for the three limit states the frictional and the frictionless soil slopes with V_S = 300 m/s and β = 40º subjected to the M2 motion.

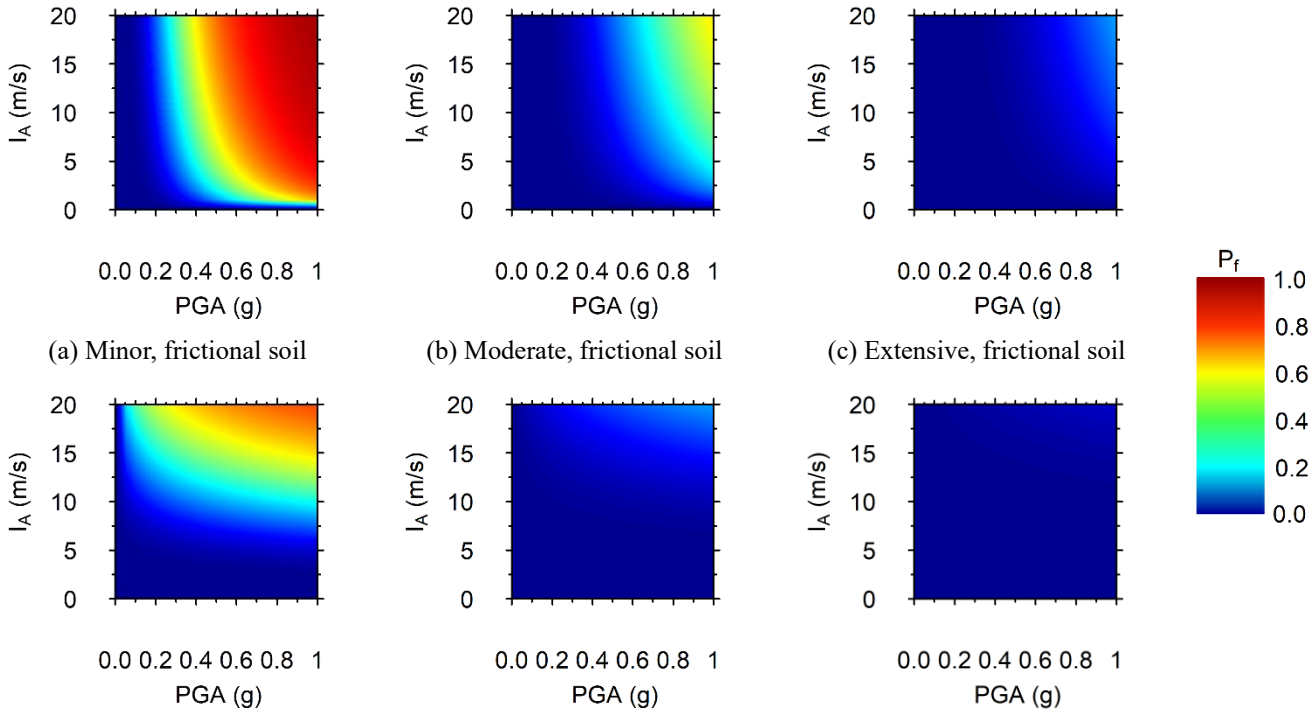

(a) Minor, frictional soil (b) Moderate, frictional soil (c) Extensive, frictional soil

(d) Minor, frictionless soil (e) Moderate, frictionless soil (f) Extensive, frictionless soil

Fig. E4 P_f for the two (PGA and I_A) for the three limit states the frictional and the frictionless soil slopes with V_S = 300 m/s and β = 20º subjected to the M4 motion.

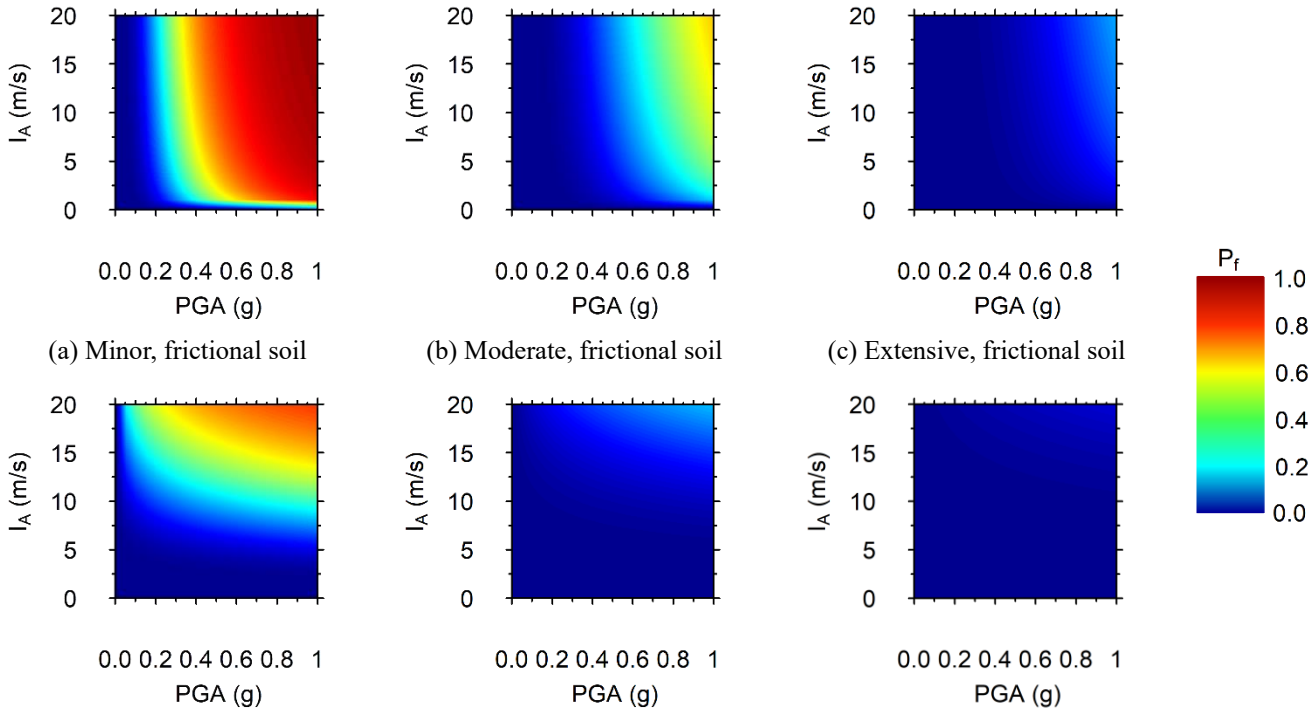

(a) Minor, frictional soil (b) Moderate, frictional soil (c) Extensive, frictional soil

(d) Minor, frictionless soil (e) Moderate, frictionless soil (f) Extensive, frictionless soil

Fig. E 5 P_f for the two (PGA and I_A) for the three limit states the frictional and the frictionless soil slopes with V_S = 300 m/s and β = 30º subjected to the M4 motion.

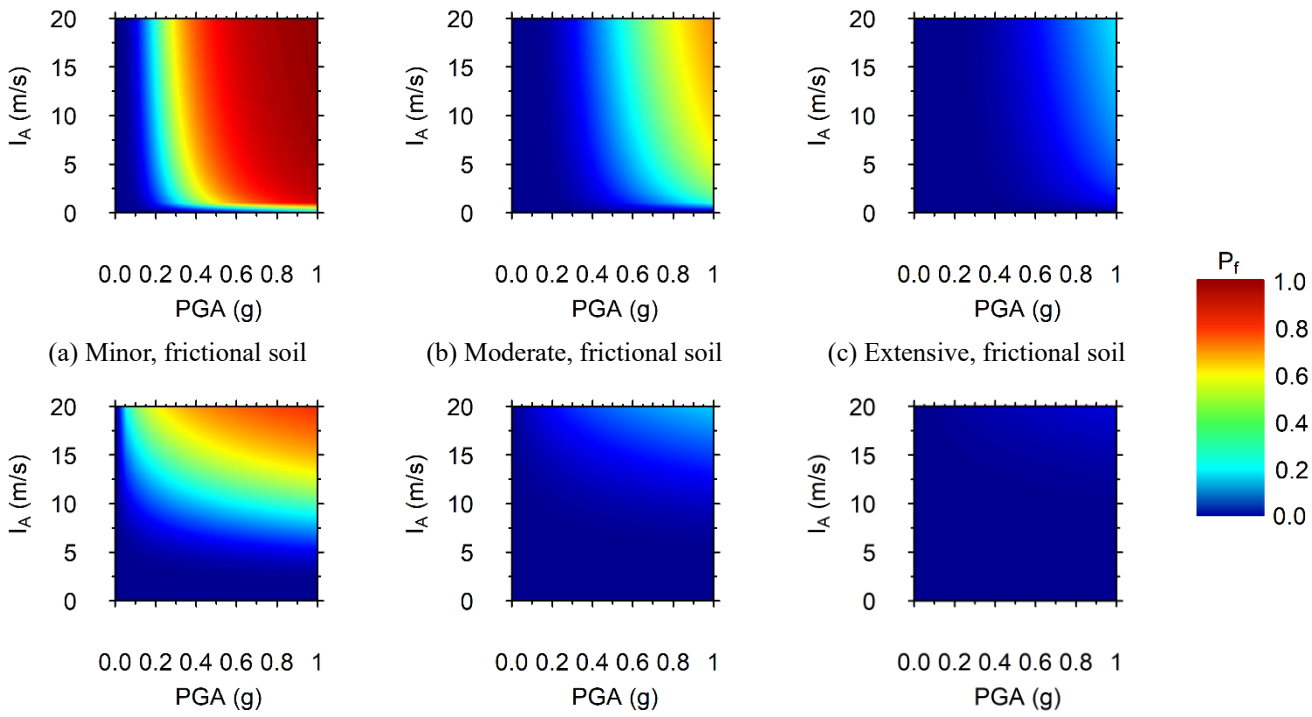

(a) Minor, frictional soil (b) Moderate, frictional soil (c) Extensive, frictional soil

(d) Minor, frictionless soil (e) Moderate, frictionless soil (f) Extensive, frictionless soil

Fig. E6 P_f with respect to the PGA and I_A for the three limit states the frictional and the frictionless soil slopes with V_S = 300 m/s and β = 40º subjected to the M4 motion